Copyright Warning & Restrictions

The copyright law of the United States (Title 17, United States Code) governs the making of photocopies or other reproductions of copyrighted material.

Under certain conditions specified in the law, libraries and archives are authorized to furnish a photocopy or other reproduction. One of these specified conditions is that the photocopy or reproduction is not to be "used for any purpose other than private study, scholarship, or research." If a, user makes a request for, or later uses, a photocopy or reproduction for purposes in excess of "fair use" that user may be liable for copyright infringement,

This institution reserves the right to refuse to accept a copying order if, in its judgment, fulfillment of the order would involve violation of copyright law.

Please Note: The author retains the copyright while the New Jersey Institute of Technology reserves the right to distribute this thesis or dissertation

Printing note: If you do not wish to print this page, then select "Pages from: first page # to: last page #" on the print dialog screen

ABSTRACT

GENERALIZED DFT:
EXTENSIONS IN COMMUNICATIONS

by
Yuewen Wang

Discrete Fourier Transform (DFT) is a restricted version of Generalized DFT (GDFT) which offers a very limited number of sets to be used in a multicarrier communication system. In contrast, as an extension on Discrete Fourier Transform (DFT) from the linear phase to non-linear phase, the proposed GDFT provides many possible carrier sets of various lengths with comparable or better performance than DFT. The availability of the rich library of orthogonal constant amplitude transforms with good performance allows people to design adaptive systems where user code allocations are made dynamically to exploit the current channel conditions in order to deliver better performance.

For MIMO Radar systems, the ideal case to detect a moving target is when all waveforms are orthogonal, which can provide an accurate estimation. But this is not practical in distributed MIMO radars, where sensors are at varying distances from a target. Orthogonal waveforms with low auto- and cross-correlations are of great interest for MIMO radar applications with distributed antennas. Finite length orthogonal codes are required in real-world applications where frequency selectivity and signal correlation features of the optimal subspace are compromised. In the first part of the dissertation, a method is addressed to design optimal waveforms which meets above requirements for various radar systems by designing the phase shaping function (PSF) of GDFT framework with non-linear phase.

Multicarrier transmission such as orthogonal frequency-division multiplexing (OFDM) has seen a rise in popularity in wireless communication, as it offers a promising choice for high speed data rate transmission. Meanwhile, high peak-to-average power ratio (PAPR) is one of the well-known drawbacks of the OFDM system due to reduced power efficiency in non-linear modules. Such a situation leads to inefficient amplification and increases the cost of the system, or increases in interference and signal distortion. Therefore, PAPR reduction techniques play an essential role to improve power efficiency in the OFDM systems. There has been a variety of PAPR reduction methods emphasizing different aspects proposed in the literature. The trade-off for PAPR reduction in the existing methods is either increased average power and/or added computational complexity. A new PAPR reduction scheme is proposed that implements a pre-designed symbol alphabet modifier matrix (SAM) to jointly modify the amplitude and phase values of the original data symbol alphabets prior to the IFFT operation of an OFDM system at the transmitter. The method formulated with the GDFT offers a low-complexity framework in four proposed cases devised to be independent of original data symbols. Without degrading the bit error rate (BER) performance, it formulates PAPR reduction problem elegantly and outperforms partial transmit sequences (PTS), selected mapping technique (SLM) and Walsh Hadamard transform (WHT-OFDM) significantly for the communication scenarios considered in the dissertation.

GENERALIZED DFT:
EXTENSIONS IN COMMUNICATIONS

by
Yuewen Wang

A Dissertation
Submitted to the Faculty of
New Jersey Institute of Technology
in Partial Fulfillment of the Requirements for the Degree of
Doctor of Philosophy in Electrical Engineering

Helen and John C. Hartmann Department of
Electrical and Computer Engineering

January 2016

.

APPROVAL PAGE

GENERALIZED DFT:
EXTENSIONS IN COMMUNICATIONS

Yuewen Wang

Dr. Ali N. Akansu, Dissertation Advisor Professor of Electrical and Computer Engineering, NJIT	Date
Dr. Ali Abdi, Committee Member Associate Professor of Electrical and Computer Engineering, NJIT	Date
Dr. Richard A. Haddad, Committee Member Professor Emeritus of Electrical and Computer Engineering, NJIT	Date
Dr. Alexander M. Haimovich, Committee Member Distinguished Professor of Electrical and Computer Engineering, NJIT	Date
Dr. Zoi-Heleni Michalopoulou, Committee Member Professor of Mathematical Sciences, NJIT	Date

BIOGRAPHICAL SKETCH

Author: Yuewen Wang

Degree: Doctor of Philosophy

Date: January 2016

Undergraduate and Graduate Education:

- Doctor of Philosophy in Electrical Engineering,
  New Jersey Institute of Technology, Newark, NJ, 2016

- Master of Science in Electrical Engineering,
  New Jersey Institute of Technology, Newark, NJ, 2009

- Bachelor of Science in Electrical Engineering,
  Shanghai Tongji University, Shanghai, P. R. China, 2006

Major: Electrical Engineering

Presentations and Publications:

Yuewen Wang, Ali N. Akansu, "Low-complexity peak-to-average power ratio reduction method for orthogonal frequency division multiplexing communications," *IET Communications*, vol. 9, no. 17, pp. 2153-2159, Nov. 2015.

Yuewen Wang, Ali N. Akansu, K. Belfield, B. Hubbi, and Xuan Liu, "Robust motion tracking based on adaptive speckle decorrelation analysis of OCT signal," *Biomedical Optics Express*, vol. 9, no. 11, pp. 4302-4316, Nov. 2015.

Yi Qiu, Yuewen Wang and Xuan Liu, "Spatially adaptive wavelet denoising for optical Doppler tomography," to be submitted to *Journal of the Optical Society of America A*, 2015.

Yuewen Wang, Ali N. Akansu, "Low-complexity peak-to-average power ratio reduction method for orthogonal frequency division multiplexing communications in Four cases," to be submitted to *Information Sciences and Systems (CISS)* 2016.

Yuewen Wang, Ali N. Akansu, and Alexander M. Haimovich, "Generalized DFT waveforms for MIMO radar," *Sensor Array and Multichannel Signal Processing Workshop (SAM)*, pp.301-304, June 2012.

Yuewen Wang and Ali N. Akansu, "Generalized DFT based partial matched filter bank for Doppler estimation," *Information Sciences and Systems (CISS)*, pp.1-6, March 2012.

谨以此论文献给我最爱的家人

To my Family

ACKNOWLEDGMENT

First of all, I want to express my sincere gratitude to my advisor, Prof. Ali N. Akansu, for his endless support, guidance, and encouragement throughout my doctoral study. Words fall short to describe the amount of effort he has put into this work which I deeply appreciate. He taught me how to be innovative, entrepreneurial, thorough, detail- and, result-oriented. I am going to miss our countless hours of discussions over coffee on exciting research as well as anything related to life in general.

I am also grateful to Prof. Alexander M. Haimovich for advising me on the research of MIMO rader; Prof. Zoi-Heleni Michalopoulou of the Mathematical Sciences Department of NJIT; also Prof. Abdi Ali and Prof. Richard A. Haddad for serving on my dissertation committee and for their continued support. I appreciate their time and their brilliant comments and suggestions. I am also greatly indebted to Prof. Xuan Liu for guiding me about her research work on speckle decorrelation analysis of OCT signals.

I also appreciate the help provided by Handan Agirman-Tosun, Onur Yılmaz, Yu Liu, Nan Wu, Shahrouz Khalili, Erjian Zhang, Yanjia Sun and other members of the Center for Wireless Communications and Signal Processing Research. I would like to thank Ms. Clarisa Gonzalez-Lenahan and the staff of the Graduate Studies office of NJIT for their reviewing of this dissertation.

Last and most especially, I would like to thank my mother, for her endless support and encouragement. I cannot stress enough how grateful I am to my mother for always being there, right next to me. Without her, this work would not have been possible.

TABLE OF CONTENTS

TABLE OF CONTENTS
(Continued)

Chapter **Page**

TABLE OF CONTENTS
(Continued)

Chapter **Page**

LIST OF TABLES

LIST OF FIGURES

LIST OF FIGURES
(Continued)

Figure **Page**

LIST OF FIGURES
(Continued)

Figure **Page**

CHAPTER 1

MOTIVATION AND OVERVIEW

1.1 Introduction

Multicarrier transmission such as orthogonal frequency-division multiplexing (OFDM) with rising popularity in wireless communication has been successfully used in various communication technologies. The OFDM system brings the advantages of avoiding frequency selective fading, narrow band interference and inter-symbol interference (ISI) [1], [2]. The easy implementation of this system, by using Fast Fourier Transform (FFT), is also quite attractive.

In this dissertation, the framework of Generalized Discrete Fourier Transform (GDFT) proposed by Prof. Ali N. Akansu and Dr. Handan Agirman-Tosun [3], [4] is introduced to communication systems. As an extension on Discrete Fourier Transform (DFT) from the linear phase to non-linear phase, several close-form phase functions of GDFT are summarized into G matrix families, through shifting the phases of the function in DFT in various ways for different purposes. Furthermore, to provide a larger research space, the amplitudes of the basis function in DFT can also be pursued. It was shown that not only is DFT a special solution of GDFT [4], but some popular orthogonal block transforms, such as Discrete Sine Transform (DST), Discrete Cosine Transform (DCT) [5], [6] and other block transforms can also be expressed within the GDFT framework with their unique full G matrices [3], [4].

It is noteworthy that infinitely possible GDFT sets are available with constant or non-constant amplitudes along with non-linear phase functions, the optimal basis

(amplitude and phase) for the desired codes of merit can be designed by exploiting different types of G matrices. The GDFT with full G matrix will be more complicated but has more freedom to exploit both in phase and amplitude spaces and brings more possibilities to design codes in various communication scenarios.

1.1.1 MIMO Radar Waveforms

With the rapid development of Multiple Input Multiple Output (MIMO) based technologies in many communications applications, MIMO radars implementing OFDM signals have also become popular in view of their ability to sense and register a target with multiple waveforms from a variety of angles. Thus, they offer improvements to detect and classify the target more accurately [7], [8].

To extract the target information, waveforms emitted by multiple antennae and returned from a target need to be separated at the MIMO radar receivers. Ideally, the waveforms should be orthogonal to each other for the purpose of decorrelation, but this condition cannot be met in the distributed MIMO radars, where sensors are at varying distances from a target. Thus, designing orthogonal waveforms with low auto- and cross-correlations are of great interest for MIMO radar applications with antennas in distributed allocations. Waveforms employed in MIMO radars should be carefully chosen in order to minimize self-interference.

For high localization resolutions, the auto-correlation functions of waveforms should have low-peak sidelobe levels in any radar system. In MIMO radars, in addition to demanding low peak sidelobes in auto-correlation functions, the cross-correlations between waveforms are also required to be low in order to detect multiple targets with high resolution. Therefore, the optimal design of orthogonal waveform sets with low

auto-correlation and low cross-correlation properties is crucial for the detection performance of MIMO radar systems.

For these techniques comprised of time and frequency domain signal processing, the *Ambiguity Function* is also very important with respect to examination on radar estimation and detection. In radar and sonar signal processing, the ambiguity function shows the distortion of the receiver matched filter's response in consequence of the time delay and Doppler shift. Time delay indicates the distance between the target and radar sensor stations while Doppler shift reflects the motion variation of the moving target. This is a two-dimensional function of time delay and Doppler frequency which is shown as [9]

$$\chi(\tau, f) = \int_{-\infty}^{\infty} s(t) s^{*}(t-\tau) e^{-j2\pi ft} dt. \tag{1.1}$$

Here τ and f denote time delay and Doppler frequency shift, respectively. A sharp delta-like ambiguity function would be the ideal case for the resolution of time delay and Doppler shift, just as in a non-interfering environment to detect the stationary target, but it's not practical in real MIMO radar systems.

In this dissertation, the phase design of the waveforms is relaxed to have non-linear phase function and forms complex orthogonal sets to pursue optimal waveforms for various radar system configurations [49]. The GDFT is used to generate optimal constant amplitude waveforms for MIMO radar applications in terms of optimizing correlation properties. These GDFT designed waveforms are shown to have lower peak-to-sidelobe ratio and better ambiguity function performance than the popular codes sets such as *Multifrequency Complementary Phase Coded* (MCPC) and *Oppermann* waveforms reported in the literatures [10], [11], [12].

1.1.2 Peak to Average Power Ratio of OFDM Signal

Presently, the phenomenon of increased demand on explosive information growth requires technologies to support high speed and quality transmissions. With the advantages of taking efficient use of the frequency spectrum, as well as providing resistant to frequency selective fading, the orthogonal frequency division multiplexing (OFDM) signals are computationally competent with the introduction of adapting its rapid algorithm, namely FFT techniques to realize the modulation and demodulation operations[13]. Therefore, OFDM signal offers a promising choice for high speed data rate transmission. On the other hand, the high peak-to-average power ratio (PAPR) of the transmitted signal is one of the major drawbacks of multicarrier transmission such as OFDM communication system.

Since the OFDM signal is a sum of orthogonal frequency modulated subcarriers, when subcarriers weighted with the corresponding symbol alphabet values are added coherently, the resulting high peak-to-average power ratio becomes a major deficiency of the OFDM systems due to reduced power efficiency and signal distortion in non-linear modules such as power amplifier (PA) and digital-to-analog converter (DAC) [14].

High peak power of OFDM frame (signal) prevents the PA from operating within its linear region, and consequently causes additional interference. It also induces bit error rate (BER) performance degradation where BER is also an important factor that is closely related to the power increase in the transmitted signal. Moreover, in order to avoid such situations, it calls for a wider dynamic range in PA and DAC to accommodate the large peaks of the OFDM frame and reduce the signal distortion because of the nonlinearity. Such a case leads to inefficient amplification and increases the cost of the system as a sacrifice. Therefore, PAPR reduction techniques play an essential role to improve power

efficiency in the OFDM systems.

A plethora of research studies on PAPR reduction techniques has been reported in the literature [15], and can be classified into different approaches including *Clipping and Filtering* [16], [17], [18], *Coding Technique* [19], [20], [21], *Selected Mapping Technique* (SLM) [22], [23], *Partial Transmit Sequences* (PTS) [24], [25], [26], *Tone Reservation* (TR) [27], [28], *Tone Injection* (TI) [29], [30] and *Active Constellation Extension* (ACE) [31], [32]. All of these techniques have their advantages and disadvantages in terms of performance distortion, average power increase, date rate reduction or considerable high computational complexity. *Clipping* does not increase the overall signal power, but results in signal distortion which leads to out-of-band interference. The *Coding Technique* without signal distortion requires low PAPR codes to be chosen but leaving the largest Hamming distances in their signaling space. The techniques of TR, TI and ACE methods all introduce the higher average power, which cause the power inefficiency.

Among these PAPR reduction methods, the techniques such as selected mapping (SLM) and partial transmit sequences (PTS) modify the phase and/or amplitude of symbols in the original symbol alphabet (SA). These two techniques are very similar in the principles which do not increase average power or signal distortion, therefore, both have been successfully used in OFDM communication systems and also popularly adapted in the MIMO-OFDM systems.

On the other hand, such methods have shortcomings of heavy computational burden and implementation costs caused by required multiple inverse fast-Fourier transform (IFFT) operations at a single transmitter. Furthermore, the side information (SI) is require to be sent to the receiver in order to retrieve the original data symbol alphabets by

getting rid of the transmitter selected phase shifting sequence set employed in the SLM and PTS methods. If the side information is received in error, the entire data block may be lost during transmission and as a consequence, it causes the degradation in BER performance. Therefore, the SLM and PTS techniques provide a good PAPR performance without signal distortion but bring high system complexity and computational cost with the data rate loss that need to reserve bits for side information.

There are a flurry of extension methods on the SLM and PTS techniques, for the purposes of eliminating SI transmission [33]-[36], or lowering system complexity [37]-[40] and so on. Some techniques may have an degradation in BER at the receiver if the transmit signal power is increased when such methods are modifying not only phase but also amplitudes on the original data symbols [38], [39], [41].

In this dissertation, a low complexity PAPR reduction method utilizing only one symbol alphabet modifier matrix and a single pair of FFT/IFFT operations is proposed which is the case of GDFT with full G matrix framework [42]. This work represents a prominent improvement in PAPR reduction that permits the reduction of the complexity and cost of the transmitter significantly. It is also shown that the SLM and PTS techniques are special cases of this proposed GDFT framework method called Symbol Alphabet Modifier Matrix (SAM).

The performance improvements of the proposed SAM method for various OFDM communication scenarios including the Space-Time Block Coding (STBC) MIMO-OFDM system are evaluated by simulation comparison on PAPR and BER performances.

1.2 Dissertation Outline

In this section, the organizations and contributions of this dissertation will be outlined.

Chapter 2: In this chapter, some famous orthogonal block transforms such as Discrete Fourier Transform (DFT) and Walsh-Hadamard Transform (WHT) used for comparisons in other chapters are introduced. The mathematical preliminaries of Generalized Discrete Fourier Transform (GDFT) which is implemented throughout the whole dissertation are stated. The different G matrix families are also summarized in terms of close form phase function representations.

Chapter 3: The method to design optimal waveforms is presented for various radar system configurations. The GDFT with nonlinear phase is used to design optimal constant amplitude waveforms with optimized correlation properties for MIMO radar applications. These waveforms are shown to have better peak-to-sidelobe ratio than the Multi-frequency Complementary Phase Coded (MCPC) and Oppermann waveforms that reported in the literature [4-6]. The presentation of ambiguity functions for different waveforms are also provided to show an outperformance of GDFT based waveforms over the others. Additionally, the Partial Matched Filter Bank [52]-[54] sampled the exponential part of the received signal in a radar system is combined with the promising correlation minimized GDFT super-frame waveforms for Doppler estimation.

Chapter 4: In this chapter, the basic and the main drawback of OFDM communications is discussed. The typical techniques for reducing Peak-to-Average Power Ratio (PAPR) are introduced to modify the original symbol alphabet through phase rotation and/or amplitude change pre- or post-IFFT operator. The representational techniques such as partial transmit sequences (PTS), selective mapping (SLM) and

Walsh-Hadamard transform (WHT) methods are explained. An extension on SLM technique is also stated for comparisons.

Chapter 5: A low-complexity PAPR reduction framework is outlined to jointly modify phase and amplitude values of the original symbols in the alphabet such as *M*-PSK and *M*-QAM. The design procedure is explained in detail. This framework utilizes only one IFFT/FFT operator pair for transmultiplexing of symbols without any SI. The merit of the proposed method to design a symbol alphabet modifier matrix (SAM) for PAPR reduction is shown through performance comparisons for the application scenarios presented in this chapter. The theoretical analysis of Bit Error Rate (BER) on AWGN and multipath Raleigh fading channels is presented in Appendix A and B. Performance and system complexity evaluations are given at the end of this chapter.

Chapter 6: The proposed symbol alphabet modifier matrix is also employed in the design of PAPR reduction for Space-Time Block Coding (STBC) MIMO-OFDM system. With the advantages of implementing SAM method and comparing it with the popularly used SLM technique, a further reduced PAPR performance is exhibited without BER degradation.

Chapter 7: Finally, the conclusions of the contributions of the dissertation and the future work are discussed in this chapter.

CHAPTER 2

MATHEMATICAL PRELIMINARIES

2.1 Orthogonal Block Transforms

The orthogonal block transforms are widely employed in multi-user communication systems and signal analysis applications. In these signal processing systems, the input signal linearly combined with each function of the block transform and assigned to each user. Among the various orthogonal transforms, the complex block transform such as Discrete Fourier Transform (DFT), Walsh-Hadamard Transform (WHT) are signal independent orthogonal transforms, all basis functions of which, as a transform matrix or codes set, are consisting of linear phases. All popular fixed length and signal independent transforms have either real value or linear phase symmetrically in their basis. In signal processing and communications, DFT successfully put in use of several applications due to its easy implementation of Fast Fourier Transform (FFT) and frequency spectrum efficiency of its perfect orthogonality.

First, the function set of the orthogonal complex function is defined as

$$\phi_k(n) = e^{j(2\pi/N)kn} \qquad k,n = 0,1,...,N-1. \tag{2.1}$$

Here N denotes the size of the orthogonal matrix or codes set. They satisfy the orthogonality condition expressed as

$$\sum_{n=0}^{N-1} \phi_k(n)\phi_l^*(n) = \sum_{n=0}^{N-1} e^{j(2\pi/N)(k-l)n} = \delta(k-l). \tag{2.2}$$

The k^{th} basis function corresponds to the k^{th} row of the DFT matrix which is shown as

$$A_{DFT} = \left[\phi_k^*(n)\right]_{DFT} = \left[e^{-j\frac{2\pi kn}{N}} \right] \quad k,n = 0,...,N-1. \tag{2.3}$$

Here, the notation (*) indicates the matrix conjugate operation. Therefore, the Inverse DFT (IDFT) is defined as

$$A_{IDFT} = \left[\phi_k^*(n)\right]_{DFT} = \left[e^{j\frac{2\pi kn}{N}} \right] \quad k,n = 0,...,N-1. \tag{2.4}$$

Accordingly, the phase function of the k^{th} basis of the DFT matrix is shown as

$$\theta_k(n) = kn, \qquad k,n = 0,1,...,N-1. \tag{2.5}$$

The constant value of $2\pi/N$ is omitted in the phase function (2.5) in order to emphasize the linearity of the function (2.4).

The discrete-time Walsh-Hadamard transform function set is composed of N orthogonal sequences, where the elements of each sequence are either +1 or -1 valued. The basis sequences of the WHT set with given length are defined as [43]

$$\begin{aligned} H_1 &= \frac{1}{\sqrt{2}}\begin{bmatrix} 1 & 1 \\ 1 & -1 \end{bmatrix} \\ H_{2N} &= \frac{1}{\sqrt{2}}\begin{pmatrix} H_N & H_N \\ H_N & -H_N \end{pmatrix} = H_N \otimes H_N, \end{aligned} \tag{2.6}$$

where the notation $\otimes$ indicates the matrix Kronecker product operator [44]. It can be observed that the Walsh-Hadamard transform have even or odd symmetry of sequences in

the time domain, according to the Fourier Transform property, they are exhibiting linear phase in the frequency domain.

2.2 Generalized Discrete Fourier Transform with Non-linear Phase

2.2.1 Introduction

The traditional DFT with linear phase is extended to explore the phase space, from linear to non-linear, as expressed in the modified transform kernel [3]

$$\begin{aligned} A_{GDFT} &= \left[\tilde{\phi}_k (n) \right]_{GDFT} \\ \tilde{\phi}_k (n) &= e^{j(2\pi/N)\varphi_k(n)n} = e^{j(2\pi/N)kn} \cdot e^{j(2\pi/N)\psi_k(n)n}, \end{aligned} \tag{2.7}$$

and the *phase shaping function* (PSF), as the exponential part of the kernel, is decomposed into two functions, one of which is the basis function of DFT, can be defined as

$$\begin{aligned} &\hat{\varphi}_k (n) = \varphi_k (n) n = kn + \psi_k (n) \\ &\psi_k (n) = \hat{\varphi}_k (n) - kn = \left[\varphi_k (n) - k \right] n \\ &k = 0,1,...,N-1, \;\; n = 1,...,N-1; \;\; \psi_k (n) \in \mathbb{R}, \;\; \hat{\varphi}_k (0) = \psi_k (0). \end{aligned} \tag{2.8}$$

The resulting orthogonal set is called the *Generalized Discrete Fourier Transform* (GDFT).

GDFT kernel offers an *uncountable set,* and therefore, there are infinitely many constant modulus sets whereas DFT basis is the unique one with the linear phase function of integer-only slopes that is $\varphi_k (n) = k, \; k \in \mathbb{Z}, \; \forall n$, and zero PSF for the set, $\varphi(n) = 0$ as

seen in (2.8). Hence, one might methodically design such GDFT sets based on performance metrics of interest.

2.2.2 GDFT Design

The GDFT in the matrix form can be written as

$$\begin{aligned} A_{GDFT} &= A_{DFT}G \quad A_{GDFT}A_{GDFT}^{-1} = I \\ A_{GDFT}^{-1} &= A_{GDFT}^{H} \quad GG^{H} = I, \end{aligned} \tag{2.9}$$

where the notation $[\cdot]^{-1}$, $[\cdot]^{*}$ and $[\cdot]^{H}$ indicates the matrix inverse, conjugate and *Hermitian* (conjugate transpose) operators, respectively, and I is used to represent the *identity matrix.*

There are several summarized G matrix families used for generating GDFT matrices.

1) Diagonal *G* Matrix Family

The diagonal elements of G matrix must be constant modulus for the orthonormal GDFT matrix in equation (2.9), and can be defined in following three forms.

Constant Valued Diagonal Elements: All elements of this diagonal matrix have the same constant amplitude complex value as expressed in

$$G(k,n) = e^{j(2\pi/N)\psi_k(n)} = \left\{ \begin{array}{cc} e^{j\theta} & k = n \\ 0 & k \neq n \\ & k,n = 0,1,...,N-1 \end{array} \right\}. \tag{2.10}$$

This type generates a phase shifted version of the A_{DFT} matrix with θ radians as the A_{GDFT} matrix. Hence, the linear phase property is still preserved in this case.

Non-constant Valued Diagonal Elements: In this case, all elements have constant amplitude, non-constant phases complex values which are defined as

$$G(k,n) = e^{j(2\pi/N)\psi_k(n)} = \begin{Bmatrix} e^{j\theta_{kk}} & k = n \\ 0 & k \neq n \\ & k,n = 0,1,...,N-1 \end{Bmatrix}. \quad (2.11)$$

The rows of A_{GDFT} are obtained as element-wise multiplication of the A_{DFT} rows with the elements of diagonal *G* matrix in this scenario. It can be observed that in the basis function of A_{DFT}, each sample is phase shifted, independent of others. On the other hand, each element in one column of A_{DFT} has the same amount of phase rotation.

Therefore, the phase function in this case of A_{GDFT} is not linear any more, but the phase difference between rows keeps the linearity.

Non-constant Two Diagonal Matrices G_1 and G_2: In this type of diagonal G matrix, a more flexible phase shaping function for GDFT is redefined in such a way as shown in the following matrix set

$$G_1(k,n) = \begin{Bmatrix} e^{j\theta_{kk}} & k = n \\ 0 & k \neq n \\ & k,n = 0,1,...,N-1 \end{Bmatrix}, \quad (2.12)$$

and another one is

$$G_2(k,n) = \begin{Bmatrix} e^{j\gamma_{nn}} & k = n \\ 0 & k \neq n \\ & k,n = 0,1,...,N-1 \end{Bmatrix}. \quad (2.13)$$

The kernel used to generate A_{GDFT} for this case becomes

$$\tilde{\phi}_k(n) = e^{j\left[(2\pi/N)kn+\theta_{kk}+\gamma_{nn}\right]} \quad k,n = 0,1,...,N-1, \tag{2.14}$$

and in the matrix form is expressed as

$$\begin{aligned} &A_{GDFT} = G_1 \cdot A_{DFT} \cdot G_2 \qquad A_{GDFT} \cdot A_{GDFT}^{*T} = I \\ &G_1 \cdot G_1^{\,H} = I \qquad\qquad G_2 \cdot G_2^{\,H} = I. \end{aligned} \tag{2.15}$$

This design method allows people to uniquely modify the elements of the k^{th} column in A_{DFT} matrix with the shifted phase θ_{kk} and n^{th} row with the shifted phase γ_{nn}.

2) Full *G* Matrix Family

In this family, the elements in the *G* matrix are constant or non-constant amplitude complex values and can be defined as

$$G(k,n) = g_{k,n} e^{j\theta_{k,n}} \qquad k,n = 0,1,...,N-1. \tag{2.16}$$

Here the amplitude is positive real value as $g_{k,n} \in \mathbb{R}^+$. The expression of A_{GDFT} is defined as

$$\begin{aligned} &A_{GDFT} = A_{DFT} \cdot G = \left[\tilde{\phi}_k(n)\right]_{GDFT} \\ &\tilde{\phi}_k(n) = g_{k,n} \cdot e^{j(2\pi/N)kn} \cdot e^{j\theta_{k,n}} \qquad k,n = 0,1,...,N-1. \end{aligned} \tag{2.17}$$

From all above definitions on the *G* matrix families of Generalized Discrete Fourier Transforms, it can be seen that Discrete Fourier Transform is a restricted solution of GDFT. It offers one and only one set in a fixed size to be used in a multicarrier communication

system. It is also highlighted that other well-known constant modulus code families such as Walsh codes [45], Oppermann codes [12] and Zadoff-Chu (ZC) sequences [46] are also the special solutions of GDFT framework [3], [4].

Furthermore, the proposed GDFT provides many possible code sets of the same and various lengths with comparable or better performance than DFT. It applies the design advantages of the non-linear phase shaping function in the GDFT framework for generating multiple OFDM frames. The availability of a rich library of such transforms exploited with good performance allows people to design adaptive systems dynamically, for the purpose of delivering better communications performance. The computational cost of Generalized Discrete Fourier Transform will be raised due to the combined implementation cost of DFT and *G* matrices. GDFT with full G matrix will be more complicated but also brings more freedom to exploit both in phase and amplitude spaces to meet different design objectives in signal processing and communication systems.

CHAPTER 3

IMPLEMENTATION IN MIMO RADARS WAVEFORMS

3.1 Correlation Performance of MIMO Radar Waveforms

In MIMO Radar systems, an orthogonal waveform set with constant modulus (amplitude) is desired to detect a moving target such that an accurate estimation can be achieved. The constant modulus property of transmitted waveforms is wanted in many radio communications systems. For such an application, the optimal subspace is the set of band-limited ideal brick-wall functions in frequency, thus all possible undesired intra- and inter-correlation terms in the signal domain are zero. Consequently, these codes are non-causal and infinitely long sequences.

In real-world applications, finite length orthogonal codes are required where frequency selectivity, auto- and cross-correlation features of the optimal subspace are compromised. For the synchronous communication environment, orthogonality is sufficiently good enough for signal decorrelation. But in distributed MIMO radars, where sensors are at varying distances from a target, the asynchronous situation destroys the strength of orthogonality for eliminating interferences. For this reason, orthogonal waveform set with low auto- and cross-correlations, which plays a crucial role, is of great interest for MIMO radar applications with distributed antennas.

3.2 Multi-frequency Complementary Phase Coded

The Multi-Frequency Complementary Phase Coded (MCPC) waveform family proposed by Nadav Levanon [10], [11] employs P4 phase sequence as its *principal phase sequence*

(*PPS*) [47], [48]. The *PPS* employs P4 codes and exhibits periodic auto-correlation properties. Further sidelobes reduction can be reached by using a train of *PPS*.

The phase sequence of the P4 code is described by [47]

$$\phi_m = \frac{\pi}{M}(m-1)^2 - \pi(m-1), \qquad m = 1,2,...M. \tag{3.1}$$

Here *M* denotes the length of the P4 sequence.

As an example, taking length $M = 5$ for all phase sequence design will be taken into consideration for the comparisons in Section 3.4.2.

Following the OFDM signal approach, *M* sequences with *M* chips (components) of each will be transmitted. The 5×5 MCPC pulse is first constructed from the length *M* sequence as the *PPS*, e.g., for length 5, $\underline{\theta}_1^T = [0, -\frac{4}{5}\pi, \frac{4}{5}\pi, \frac{4}{5}\pi, -\frac{4}{5}\pi]$. Levanon uses the cyclically left shifted version of *PPS* to generate four other phase sequences. The rest of them are calculated as

$$\begin{aligned}
\underline{\theta}_2^T &= [-\frac{4}{5}\pi, \frac{4}{5}\pi, \frac{4}{5}\pi, -\frac{4}{5}\pi, 0], \\
\underline{\theta}_3^T &= [\frac{4}{5}\pi, \frac{4}{5}\pi, -\frac{4}{5}\pi, 0, -\frac{4}{5}\pi], \\
\underline{\theta}_4^T &= [\frac{4}{5}\pi, -\frac{4}{5}\pi, 0, -\frac{4}{5}\pi, \frac{4}{5}\pi], \\
\underline{\theta}_5^T &= [-\frac{4}{5}\pi, 0, -\frac{4}{5}\pi, \frac{4}{5}\pi, \frac{4}{5}\pi].
\end{aligned} \tag{3.2}$$

Therefore, the *Original Phase Sequence Set (OPSS)* matrix in MCPC codes is populated in

$$\Theta^{OPSS} = \left[\Theta(k,n)\right] = \left[\underline{\theta}_1, \underline{\theta}_2, \underline{\theta}_3, \underline{\theta}_4, \underline{\theta}_5\right]^T \tag{3.3}$$

The typical auto-correlation of a P4 pulse exhibits a narrow main lobe at zero delay.

3.3 Oppermann Codes

Oppermann waveforms are a family of constant modulus orthogonal function set with a wide range of correlation properties, and are also considered another type for radar waveforms in correlation property comparison in this chapter. It has been shown that the well-known Zadoff-Chu sequences [46] are the special case of the Oppermann code family.

The Oppermann code contains three parameters $\{m, p, n\}$ in their kernel [12] and is described by

$$A_{OPP}(k,i) = (-1)^{ki} \exp\left(\frac{j\pi\left(k^m i^p + i^n\right)}{M}\right), \quad k,i = 1,...,M, \tag{3.4}$$

where k is an integer in the range of $[1, N)$ and prime to N. It was proven that the Oppermann codes are orthogonal only for the case of $p = 1$, and m is any positive nonzero integer number. Meanwhile, all the functions in the set A_{OPP} have the same auto-correlation magnitudes and differed only in phases [12].

3.4 Generalized DFT Waveforms for MIMO Radar

GDFT kernel suggests an uncountable set, and accordingly, there are infinitely many constant modulus GDFT sets whereas DFT basis only has linear phase functions of integer

slopes. The correlation property of these sets are different in the time and frequency domains [49]. Herein, the method which takes the advantage of the flexible phase space is presented by designing the PSF of GDFT framework with non-linear phase. The GDFT framework is employed for MIMO radar waveforms in the generation of complex orthogonal function sets with optimized auto- and cross-correlation properties.

In this section, it is shown that the MCPC waveform family can be expressed as a special case of the proposed GDFT waveforms. The length-M MCPC code is presented as an example of the proposed method as follows.

As mentioned in Section 3.2, the *Original Phase Sequence Set (OPSS)* matrix Θ^{OPSS} is populated. Then, shuffling and disturbing the orders of the original rows in Θ^{OPSS} results in a *Phase Sequence Ses (PSS)* $\Theta^l = \left[\Theta(k^l, n)\right]$, where its rows are labeled by $k = 1, 2, ..., M$, and the superscript $1 \le l \le M!$ is the index corresponding to a unique row order of a *PPS* matrix. The *OPSS* is indexed as $l = 1$ that is $\Theta^1 = \Theta^{OPSS}$. Finally, an 5×5 MCPC signal train set has a total of 5 factorial different permutations.

Next, the OFDM waveform matrix is generated as the exponent function of Θ^l and defined as $S^l = e^{j\Theta^l}$, each row of which mapping onto the subcarriers by inverse DFT and consequently, generating up to *M* OFDM frames. The k^{th} row of the exponent function S^l is written as

$$(\underline{s}_k^l)^T = \left[\exp\left(j\theta_k^l\right)\right] \quad k = 1, 2, ..., M, \tag{3.5}$$

where $(.)^T$ represents the transpose operation.

Now, define the following GDFT diagonal *G* matrix as

$$G_k^l = I\,\underline{s}_k^l, \tag{3.6}$$

that leads to the GDFT framework, or in other words, the OFDM frames stated as

$$A_{GDFT}^{k,l} = F_k^l = A_{DFT}^{-1} G_k^l \quad k = 1,2,...,N. \tag{3.7}$$

The k^{th} OFDM frame denoted as f_k^l, is the k^{th} row of GDFT set F_k^l. In the MCPC example here, $N = M = 5$.

Finally, the resulting l^{th} MCPC MIMO radar waveform is expressed as a sum of all OFDM frames as follows

$$x^l(n) = \sum_{k=1}^{5} f_k^l(n) \quad (\underline{x}^l)^T = [x^l(n)] \quad n = 1,2,...,N. \tag{3.8}$$

It is noted that the GDFT framework expressed MCPC in (3.8) offers additional waveform options with the same correlation performance since $1 \le l \le 5!$.

Now, the design of GDFT waveforms is described in detail, and they are coupled with the MCPC family. Several phase sequences of MCPC waveforms of length $N = 5$ in (3.6) is placed in a larger size diagonal matrix of GDFT framework as follows

$$G_{N^2 \times N^2}^l = \begin{pmatrix} [G_1^l] & [0] & [0] & [0] & [0] \\ [0] & [G_2^l] & [0] & [0] & [0] \\ [0] & [0] & [G_3^l] & [0] & [0] \\ [0] & [0] & [0] & [G_4^l] & [0] \\ [0] & [0] & [0] & [0] & [G_5^l] \end{pmatrix} \tag{3.9}$$

where $G^{l}_{N^2\times N^2}$ is equal to *G* as shown in equation (2.11). This representation simply links MCPC and GDFT waveform families together.

3.4.1 Optimization Metrics of Waveform Design

In this design method, the $G^{l}_{N^2\times N^2}$ matrix of (3.9) is optimized, namely *G* matrix of GDFT as expressed in (2.9) and (2.12), by a proper numerical search method in order to minimize auto- and cross-correlations peak sidelobes of the resulting MIMO waveforms for the single and multi-antenna radar scenarios as follows. The software tool to be used is called '*fminsearch*' in Matlab for this optimization task. The following metrics defined in terms of the aperiodic correlation function are utilized for optimization objectives.

a) RMS of auto-correlation sidelobes (RMS_{ac})

The auto-correlation function of a sequence X^{l} is expressed as

$$R_{X^lX^l}(i)=\sum_{k=0}^{N-i-1}X^{l}(k)X^{l^*}(k+i)\quad 0\le i\le N-1, \tag{3.10}$$

where X^{l} is any function (row) of the orthonormal GDFT matrix and that is taken as one of the OFDM fames (waveforms). The value of *i* denotes the time delay of the correlations.

Note that the auto-correlation of orthogonal constant modulus sets are the same for all basis functions. Now, the criterion to search for GDFT set of size $N\times N$ with minimized Root Mean Square (RMS) of the auto-correlation sidelobes is expressed as

$$RMS^{l}_{ac}=\left(\frac{1}{N}\sum_{i=1}^{N-1}R^{2}_{X^lX^l}(i)\right)^{\frac{1}{2}}. \tag{3.11}$$

b) RMS of cross-correlation sidelobes (RMS_{cc})

The cross-correlation function of a pair of sequences X^l and X^m is expressed as

$$R_{X^l X^m}(i) = \sum_{k=0}^{N-i-1} X^l(k) X^{m*}(k+i) \quad 0 \le i \le N-1, \tag{3.12}$$

where X^l and X^m are any two functions (rows) of the orthonormal GDFT matrix. Similarly, the criterion to search for GDFT set of size $N \times N$ with minimized RMS of the cross-correlation sidelobes is described as

$$RMS_{cc}^{l,m} = \left(\frac{1}{N} \sum_{i=1}^{N-1} R_{X^l X^m}^2(i) \right)^{\frac{1}{2}}. \tag{3.13}$$

These two optimization metrics are employed in GDFT waveform design examples for various correlation performance comparisons. It can be realized that these two criterion RMS_{ac}^l and $RMS_{cc}^{l,m}$ are functions of $\psi_k(n)$ in (2.8). Therefore, the design problem can be simply and directly reduced to the issue of optimization on phase shaping function, $\psi_k(n)$, of the GDFT in order to minimize RMS_{ac}^l and/or $RMS_{cc}^{l,m}$ defined in (3.11) and (3.13). Different weights put on the auto- and cross-correlation can be designed that depending on various scenarios and application requirements, different emphases given on auto- and cross-correlation is optional.

3.4.2 Correlation Performance Comparisons

The optimal parameters $\{m,n\}$ of Oppermann codes that minimized RMS_{ac}^l of equation

(3.8) are searched. The 5-tap optimal Oppermann codes with the corresponding set $\{m = 0.5805, p = 1, n = 2.9079\}$ is obtained by using toolbox '*fminsearch*' in MATLAB which is Nelder-Mead Simplex Algorithm based [50]. Similarly, the optimized parameter set $\{m = 5.1606, p = 1, n = 1.2880\}$ gives the minimum $RMS_{cc}^{l,m}$ of equation (3.13).

Figure 3.1 displays the auto-correlation functions of GDFT waveforms designed based on minimization of the given auto-correlation metric of (3.11) along with MCPC and Oppermann codes. Table 3.1.a tabulates the values of optimal phase sequences used in this case.

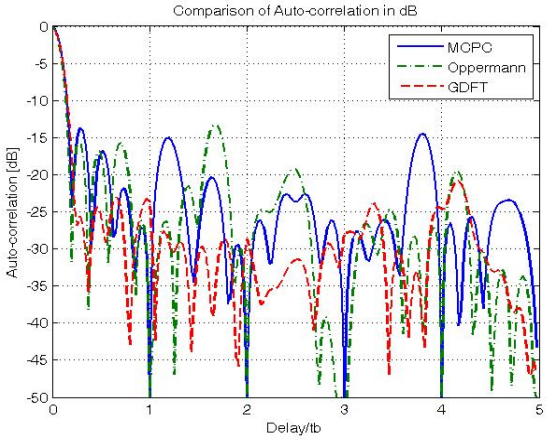

Figure 3.1 Auto-correlation functions of GDFT (RMS_{ac}^{l} based), MCPC and Oppermann waveforms (RMS_{ac} based) for N=5.

It can be observed from Figure 3.1 that the blue curve denoted for MCPC waveform displays a periodic auto-correlation property, but some of its sidelobes reaches -15 dB, while Oppermann code has an approximately peak sidelobe value of -13 dB. In contrast, the highest sidelobes of GDFT waveforms is much lower and around -25 dB.

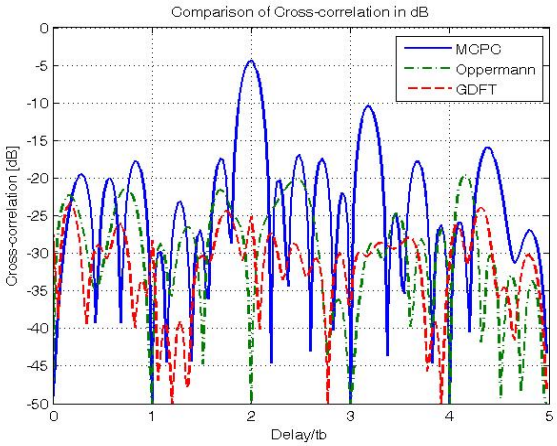

Figure 3.2 Pair-wise cross-correlations of GDFT ($RMS_{cc}^{l,m}$ based), MCPC and Oppermann waveforms (RMS_{cc} based) for N=5.

Similarly, Figure 3.2 displays the cross-correlations of GDFT based on the minimization of cross-correlation metric of (3.13) with the phase sequences tabulated in Table 3.1.b, along with the examples of MCPC for the sequence orders of {1,2,3,4,5} and {3,4,5,1,2}[10], [11], and the Oppermann waveform families considered. Significantly, GDFT waveform outperforms MCPC and Oppermann ones and constrains the sidelobes below -25 dB, whereas MCPC presents the peak value at -5dB and the Oppermann is around -20 dB for the cases [51].

The sidelobes of auto- and corss-correlation of GDFT proposed, MCPC and Oppermann based waveforms are compared in Table 3.2 in terms of the criterion given in root mean square of auto- and cross-correlation sidelobes.

Table 3.1.a Phase Sequence Set of Diagonal $G_{25\times25}$ Matrix Optimized Based on RMS_{ac}^{l} and $\Theta(k^{l},n)\in[-\pi,\pi]$

$\underline{\theta_1^l}$	$\underline{\theta_2^l}$	$\underline{\theta_3^l}$	$\underline{\theta_4^l}$	$\underline{\theta_5^l}$
0.0049	0.2069	-2.0727	-1.1614	2.9697
-1.1563	-0.0701	-1.9514	-2.1261	-1.0947
-3.0906	-1.2493	-0.4423	-0.6024	-0.3054
-0.0296	0.9166	-2.5216	0.8718	0.0502
2.2087	2.9952	1.7669	-2.3486	-2.2989

Table 3.1.b Phase Sequence Set of Diagonal $G_{25\times25}$ Matrix Optimized Based on $RMS_{cc}^{l,m}$ and $\Theta(k^{l},n)\in[-\pi,\pi]$

$\underline{\theta_1^l}$	$\underline{\theta_2^l}$	$\underline{\theta_3^l}$	$\underline{\theta_4^l}$	$\underline{\theta_5^l}$
2.5937	1.5587	0.1340	-0.1980	-1.4230
-1.0988	2.4046	1.5025	-0.9587	1.9019
1.5911	-2.9088	-2.5797	-2.6627	-1.0022
-0.2508	-2.0277	-0.1217	0.4614	-2.4405
-2.0413	0.4505	1.0868	0.8109	1.5327

Table 3.2 Auto- and Cross-Correlation Sidelobe Comparisons (in *RMS*) of GDFT, MCPC and Oppermann Waveforms for N=5

(normalized)	RMS_{ac}^{l}	$RMS_{cc}^{l,m}$
GDFT	0.0375	0.0314
MCPC	0.0770	0.1482
Oppermann	0.0725	0.0477

Figures 3.3.a, 3.3.b and 3.3.c display the corresponding ambiguity functions [9] introduced in Section 1.1.1 with respect to correlation performance of the MCPC, Oppermann and GDFT waveforms (RMS_{ac}^{l} and $RMS_{cc}^{l.m}$ based individually) for the size of OFDM super-frame as $N=M^{2}=25$.

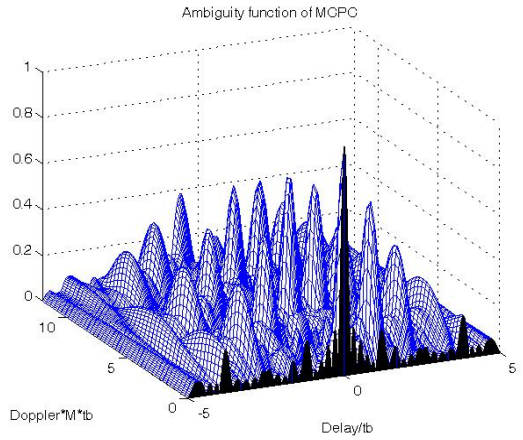

Figure 3.3.a Ambiguity function of MCPC waveforms for N=25.

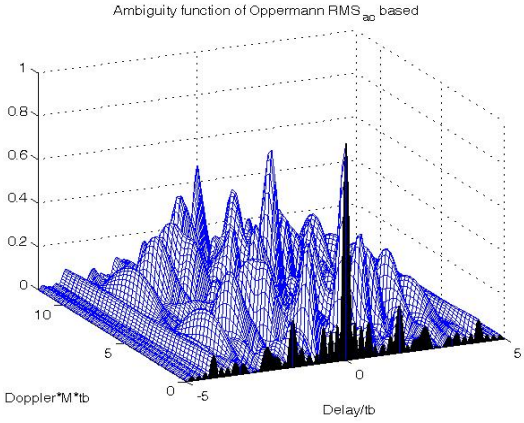

Figure 3.3.b Ambiguity function of Oppermann waveforms (RMS_{ac}^{l} based) for N=25.

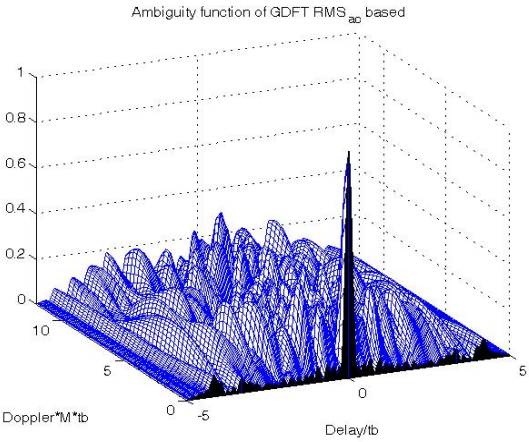

Figure 3.3.c Ambiguity function of GDFT waveforms ($RMS_{cc}^{l,m}$ based) for N=25.

It is observed from these performance comparisons that GDFT based waveforms significantly outperform MCPC and Oppermann families with respect to all metrics considered in this section. In GDFT, the entire phase space of constant modulus orthogonal basis has the freedom to be thoroughly exploited for the optimization of waveforms. Note that GDFT set has uncountable waveform designs that depends on different criteria and it provides many possible waveforms of good quality.

Moreover, it is shown that popular waveforms like MCPC and Oppermann types are the special cases of the GDFT family. The design examples presented can be extended to much larger values of N. It is expected to see better performance of GDFT based waveforms implemented in future radar systems.

3.5 Generalized DFT Based Partial Matched Filter Bank for Doppler Estimation

Partial Matched Filter Bank (PMFB) with orthogonality is a method to sample the phase functions of the received radar signals offering robust Doppler tolerance. Generalized Discrete Fourier Transform (GDFT) with nonlinear phase functions provides engineering flexibility over the traditional Discrete Fourier Transform (DFT). The design freedom of exploiting the entire phase space of constant modulus orthogonal basis brings significant values for the minimization of waveform auto- and cross-correlations that is not possible in the DFT set. In this section, utilization of GDFT waveforms with optimized correlations in a PMFB framework is proposed. It is shown that GDFT based PMFB performs quite promising for Doppler estimation in radar systems [55].

In radar systems, range delay bears information for the distance of the target, and Doppler shift represents the speed of its movement. In an ideal situation where codes are of

infinite length, orthogonal waveforms may simultaneously offer perfect auto- and cross-correlation properties. In practice, perfect correlations are not available due to the limits of implementation and various disturbances including channel noise, target movements and others.

For target detection with high range resolution, the auto-correlation functions of waveforms are required to have low sidelobe levels [11]. Furthermore, the waveform cross-correlations are desired to be low in the case of multiple antenna systems.

The design of constant modulus waveform sets with low auto- and cross-correlations is important for performance improvements in MIMO radar systems which has been discussed in Section 3.4 by employing the introduced Generalized Discrete Fourier Transform (GDFT) framework to optimize waveforms with respect to correlations where non-linear phase provides more freedom compared to the traditional DFT with linear phase [2].

Partial Matched Filter Bank (PMFB) with orthogonality and constant modulus properties facilitates an efficient method to sample the exponent function of the received signals, basically the phase, that convey inherent Doppler information. The use of GDFT with minimized correlations in PMFB presents an easy way to estimate Doppler in radar systems with a high level of accuracy.

3.5.1 Partial Matched Filter Bank

A Partial Matched Filter Bank (PMFB) to improve Doppler tolerance was proposed in [52-54]. In this method, the transmitted waveform $\underline{U}_{1\times PN}^{T}$ is a super-frame of aggregated P orthogonal frames (sub-pulses) with length N where each as expressed in a vector form

$\underline{U}_{1\times PN}^{T} = [\underline{u}_1^T, \underline{u}_2^T, ..., \underline{u}_P^T]$. Those P frames are chosen from the rows of a constant modulus, $N \times N$ orthogonal matrix where $P \le N$.

At the receiver, the received constant modulus waveform (super-frame) with the Doppler shift of f_d is formulated in the time domain as $u(n, f_d) = u(n)e^{j2\pi f_d n}$, $n = 0,1,...,NP-1$. A bank of P partial matched filters is constructed at the receiver for Doppler estimation where each filter corresponds to one of the P orthogonal frames in the transmitted super-frame.

Note that the breaking of a single match filter (super-frame) into its orthogonal building blocks (frames), and processing partial segments of the super-frame independently provides a convenient way to sample the Doppler phase at the detector. This is due to the fact that the frames are constant modulus and orthogonal.

It is emphasized that the Doppler phase sampling interval in the exponent of the received signal is defined by the dimensionality of the $N \times N$ orthogonal set. Figure 3.4 displays the block diagram of a Partial Matched Filter Bank along with filter outputs in magnitude domain.

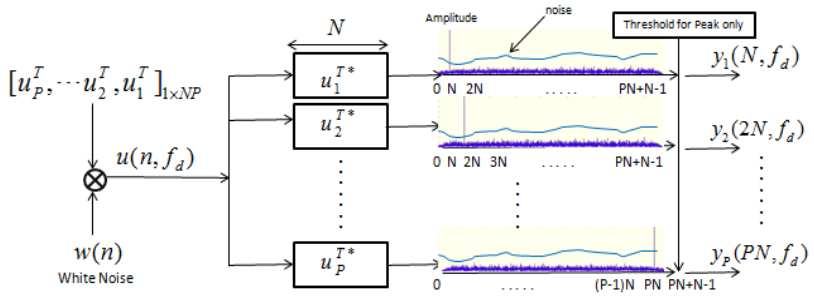

Figure 3.4 Block diagram of Partial Matched Filter Bank and filter outputs in magnitude**.**

3.5.2 GDFT Based Method for Doppler Estimation

The received signal goes through matched filters of PMFB as depicted in Figure 3.4. The transmitted super-frame may be comprised of a subset or the entire set of the GDFT basis functions of size *N*, and as an example, optimized with respect to RMS_{ac}. Hence, in addition to the additive white Gaussian noise $w(n)$ of the channel, filter outputs are dictated by the auto-correlation and cross-correlation functions of the orthonormal GDFT set employed in the transmitted waveform.

A bank of thresholds is utilized at filter outputs to locate sampling points in time. Then, the corresponding phase estimates are measured in order to obtain the Doppler information of interest as expressed in $y_p(pN, f_d) = e^{j\tilde{\psi}_D(pN)}$, $p = 1,2,...,P$. The estimated Doppler phase samples $\tilde{\psi}_D(n)$ with the sampling interval of *N* chip durations are easily calculated from samples of filter outputs as $\widetilde{\psi}_D(n) = \ln[y_p(n, f_d)],\ n = 0,1,...,NP + N - 1$.

Suppose that the received waveform $\underline{U}^T_{1\times PN}$ has detected a moving object with a Doppler shift of f_d, then, one can easily calculate $\widetilde{\psi}_D(pN) = \ln[y_p(pN, f_d)]\ \ p = 1,2,...,P$. The received phase signal samples measured as filter outputs of PMFB are displayed for the cases of $f_d = 1,2,3,4,5.5,6.5,7.5,8.5$ Hz, *P*=256, *N*=512 in Figure 3.5. Note that one can efficiently estimate Doppler shifts through calculating the slope of the two consecutive estimated phase samples for the case of constant slope in time.

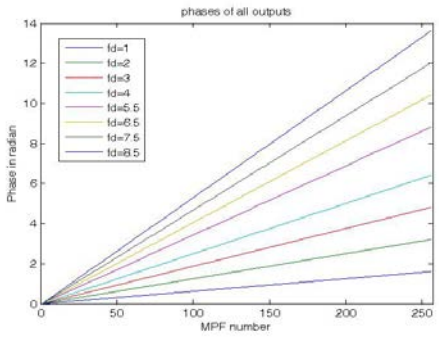

Figure 3.5 Sampled exponent function of filter outputs in a PMFB for various constant Doppler frequencies.

3.5.3 Implementation in Multiple Antenna System

In a multiple antenna system, multiple super-frames co-exist in the same channel. Therefore, their orthogonality and correlation properties need to be considered in such a system. Hence, the single antenna case is extended as presented in Section 3.5.2 for this case where the correlation measurements in the optimized design become more involved as expected.

As an example, the system here is focused on the two-antenna case where each waveform of length N^2 is comprised of the aggregated rows of a size $N \times N$ GDFT matrix. Now, two of such matrices are needed. In addition to minimization of their individual auto- and cross-correlations, these two super-frames need to have their pair-wise cross-correlations.

Note that one can create multiple super-frames when $P < N$. The trade-off is the fact that these super-frames will have their cross-correlations completely generated by auto-correlation of building orthogonal frames. Naturally, this leads to a cross-correlation sequence that is not very desirable.

Figures 3.6 and 3.7 present auto-correlation and cross-correlation sequences of super-frame examples where $N = P = 5$. A super-frame waveform of length N^2 is examined in each figure. Each case is generated from an independently optimized 5×5 GDFT matrix (two matrices in Figure 3.7 examples) based on the corresponding correlation metric. Table 3.3 provides the values of phase shaping functions in GDFT base super-frame waveforms that are optimized based on the Root Mean Square of auto-correlation, cross-correlation and a combination of these two metrics as defined in Section 3.4.1.

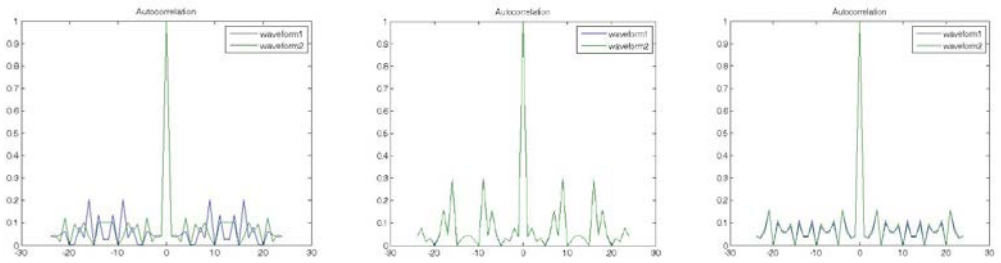

(a) (b) (c)

Figure 3.6 Auto-correlations of super-frames generated from GDFT with minimized correlation metrics of a) RMS_{ac}, b) RMS_{cc}, and c) $RMS_{ac} + RMS_{cc}$.

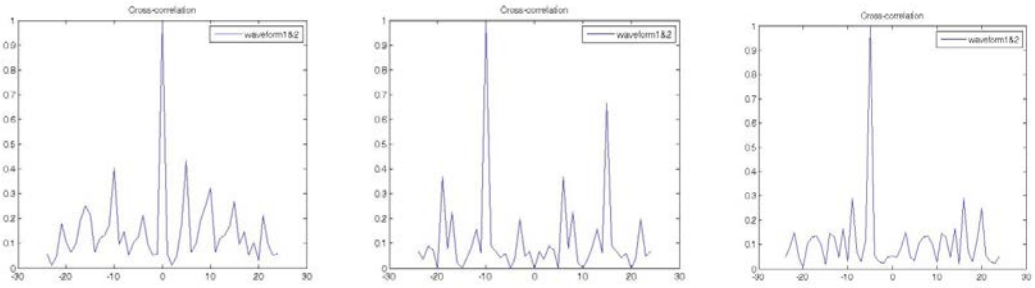

(a) (b) (c)

Figure 3.7 Pair-wise cross-correlations of super-frames generated from GDFT with minimized correlation metrics of a) RMS_{ac}, b) RMS_{cc}, and c) $RMS_{ac} + RMS_{cc}$.

Table 3.3.a Phase Shaping Functions of the Optimal Design Example Based on Minimized RMS_{ac} in Radians

1st Waveform	0.9823	-0.9701	-1.0469	-0.7767	-2.6426
2nd Waveform	1.3723	0.4248	-0.5226	1.6714	-2.4176

Table 3.3.b Phase Shaping Functions of the Optimal Design Example Based on Minimized RMS_{cc} in Radians

1st Waveform	-1.2951	1.2035	-0.2928	1.0929	-1.5163
2nd Waveform	-1.5616	-1.57628	0.6972	-0.4302	0.7304

Table 3.3.c Phase Shaping Functions of the Optimal Design Example Based on Minimized $RMS_{ac} + RMS_{cc}$ in Radians

1st Waveform	0.0112	2.9499	0.7756	-0.1637	0.0671
2nd Waveform	-1.5711	0.0976	2.7613	0.7539	-0.2586

The optimal waveform design examples show that the joint correlation metric $RMS_{ac} + RMS_{cc}$ leads to superior auto- and cross-correlations in the case of two antennas. Also note that the longer waveform length offers better correlation properties for all the cases considered in the section.

CHAPTER 4

PAPR REDUCTION METHODS FOR OFDM COMMUNICATIONS

Presently, the multicarrier transmission such as orthogonal frequency-division multiplexing (OFDM) has rising popularity in wireless communication, with advantages of making efficient use of the frequency spectrum, providing strong resistance to frequency selective fading than single carrier systems, offering computationally efficient by the introduction of FFT techniques that implement the modulation and demodulation functions [1], [2]. Furthermore, an OFDM system also provides the properties that can be against narrow band interference and Inter-Symbol-Interference (ISI). Orthogonality in frequency domain also ensures to mitigate Inter-carrier Interference (ICI) between carriers and subchannels.

On the other hand, the high peak-to-average power ratio (PAPR) is one of the well-known drawbacks of OFDM systems since the OFDM signal is a sum of orthogonal frequency modulated subcarriers. When subcarriers weighted with the corresponding symbol values are added coherently, the resulting PAPR is high, which leads to serial issues.

In order to achieve maximum efficiency, the power amplifier (PA) should preferably operate near the saturation region so that sufficient transmission power is offered. Large peaks in instantaneous signal power will induce in-band and out-band interferences, so the transmitter power amplifier must avoid nonlinearities that causes the corruption of the transmitted signal, and reduces PA’s power efficiency. Due to the existing large peaks of the OFDM signal, it cannot operate in a linear region and will

introduce additional interference into the system, which leads to an increasement of BER [56]. To avoid this, one has to increase the cost of PA's power range as the compensation. The non-linear digital-to-analog converter (DAC) module faces similar situations. Either the inefficiency power transmission cost of non-linear modules or increased interferences caused by signal distortions becomes the main deficiency of OFDM signals. These problems calls for a variety of research activities on PAPR.

4.1 OFDM System Structure and PAPR

An OFDM frame is generated by multiplexing independent symbols modulated with orthogonal frequency subcarriers. The incoming data bit stream is modulated into a sequence of symbols from the predefined symbol alphabet constellations of *M*-ary Phase-Shift Keying (*M*-PSK) or *M*-ary Quadrature Amplitude Modulation (*M*-QAM) that populate the symbol vector $\underline{X} = [X(0), X(1), ..., X(N-1)]^T$, where $[\cdot]^T$ denotes a transpose operator, *N* is the number of subcarriers employed. *M* is the power of 2 such as 4 (QPSK), 8 (8-PSK), 16 (16-QAM), and others. The continuous-time baseband multicarrier signal is the summation of *N* subcarriers weighted by symbols and expressed as [15]

$$x(t) = \frac{1}{\sqrt{N}} \sum_{k=0}^{N-1} X(k) e^{j2\pi f_k t}, \quad 0 \le t < Nt_s. \tag{4.1}$$

Subcarriers are orthogonal where $f_k = k\Delta f$, $\Delta f = 1/Nt_s$, t_s is the symbol period and $j = \sqrt{-1}$. Then, the discrete-time OFDM frame is the sampled version of (4.1) at the *Nyquist rate* $t = nt_s$ and written as

$$x(n) = \frac{1}{\sqrt{N}} \sum_{k=0}^{N-1} X(k) e^{j\frac{2\pi kn}{N}}, \quad n = 0,1,...,N\text{-}1. \tag{4.2}$$

Let $\underline{x} = \left[x(0), x(1), ..., x(N-1) \right]^T$ denote the resulting discrete-time OFDM frame in a vector form. The PAPR of an OFDM frame due to signal amplitudes fluctuation is defined as

$$\text{PAPR} = \frac{\max_{n=0,1,...,N-1} \left| x(n) \right|^2}{E\left[\left| x(n) \right|^2 \right]}, \tag{4.3}$$

where $E[\cdot]$ denotes the expectation operator.

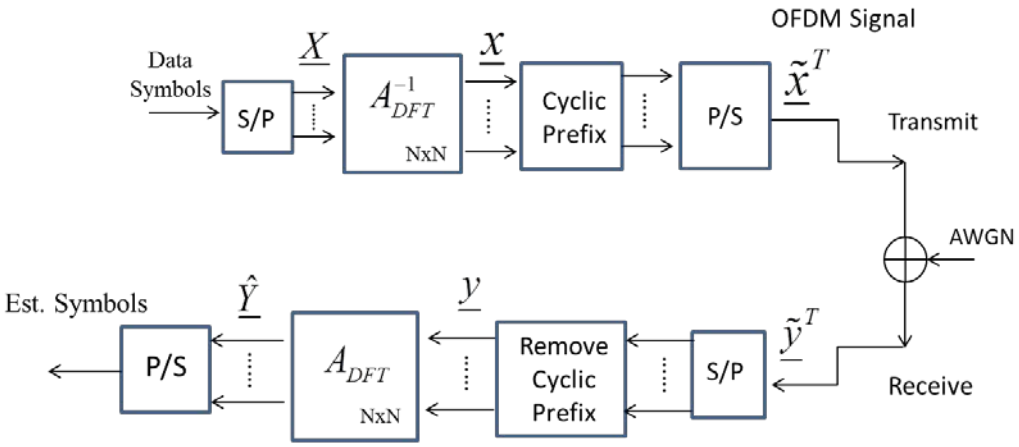

Figure 4.1 Block diagram of the OFDM communication system.

Figure 4.1 displays the block diagram of the traditional OFDM system. The *complementary cumulative distribution function* (CCDF) is a commonly used measure to evaluate PAPR performance [57]. The CCDF of the PAPR indicates the probability that the PAPR of a signal exceeds a given threshold, i.e. $\Pr\{\text{PAPR} > \text{PAPR}_0\}$.

4.2 Popular PAPR Reduction Method

There has been a variety of PAPR reduction methods emphasizing different research aspects proposed in the literatures [15]. One typical technique modifies the original symbol alphabet through performing phase rotation and/or an amplitude change pre- or post-IFFT operator in order to reduce PAPR. Representational techniques such as selective mapping (SLM) [22], [23], partial transmit sequences (PTS) [24], [25], [26], and Walsh-Hadamard transform (WHT) [43] methods have been widely used for such a task.

Although the SLM and PTS methods provide PAPR reduction, their computational complexity and the cost of utilizing multiple IFFT operators are relatively high. In addition, for a set of OFDM signal candidates used in the SLM and PTS methods, bits of side information (SI) represented in the index of the selected one must be transmitted error-free along with the OFDM frame in the system for recognition by the receiver. Due to these shortcomings, there are extensions of SLM [33]-[39] and PTS [36], [40] that also modify power levels of symbols in the alphabet in order to reduce PAPR [37], [38], [41] or to eliminate SI [33-36]. The WHT method improves PAPR without any power increase and no side information is required in a low-complexity system, but it offers less PAPR reduction compared to the SLM and PTS methods [40].

4.2.1 Selective Mapping Technique and Extensions

The basic principle of SLM is based on a type of probabilistic algorithm that generates several OFDM signal candidates represented same information. It then selects the one with the lowest PAPR for transmission, thereby statistically reducing the possibility of high PAPR. The SLM technique avoids signal distortion at the cost of some redundant searching. For implementation, each of these OFDM signal candidates is generated as a

product of original symbols multiplied subcarrier-wise with one of the randomly populated phase shifting sequences denoted as $\underline{B}^u$. This results in total U phase rotated data vectors along with U IFFT blocks, therefore it needs $\log_2 U$ bits of side information. The procedure is presented in Figure 4.2, where each phase sequence is a vector $\underline{B}^u = [\mathrm{b}_0^u, \mathrm{b}_1^u, ..., \mathrm{b}_{N-1}^u], u = 0,1,...,U-1$, $\mathrm{b}_k^u = e^{j\psi_k^u}$ and $\psi_k^u \in [0, 2\pi)$. For simplification, the researcher could randomly choose the phase set $\psi_k^u \in \{\pm\pi/2, \pm\pi\}$. After applying individual IFFT, the OFDM signal candidate becomes:

$$x^u(n) = \frac{1}{\sqrt{N}} \sum_{k=0}^{N-1} X_k b_k^u \cdot e^{j2\pi kn}, \quad n = 0,1,...,N\text{-}1, u = 0,1,...,U-1 \tag{4.4}$$

SLM makes the selection judgment of best PAPR performance sequence after going through the entire set of IFFT blocks, where the same number of IFFT blocks are required for all data streams. As a consequent, this causes a high cost and computational complexity accordingly.

When signal length N is 64, SLM technique produces the candidates takes U=8 IFFT blocks as example. The side information at least $\log_2 U$=3 bits is demanded for the purpose of recovering the signal, but errors happen when SI is lost and mistakenly determined by the receiver. Intuitively, the more signal candidates to choose from, the better PAPR performance can be reached due to the probabilistic nature. But it should be noted that large SI bits are unwanted and impractical when considering the cost of IFFT blocks. In general, SLM technique could be used to reduce PAPR efficiently, however, it causes BER degradation and applying many IFFT blocks is cumbersome.

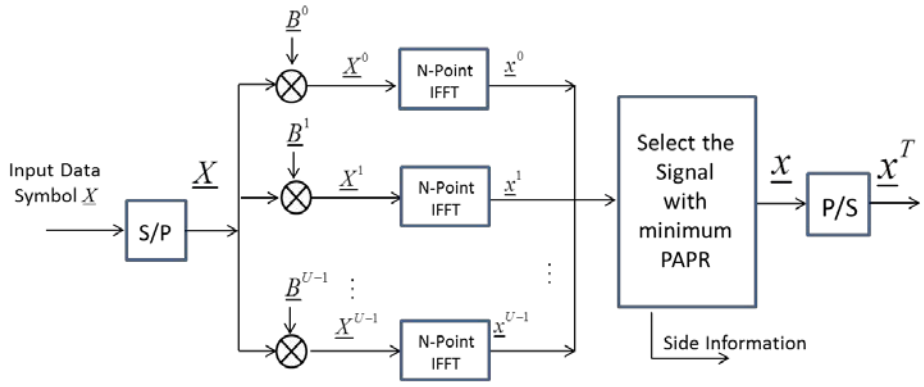

Figure 4.2 Block diagram of the SLM technique in the OFDM communication system.

With the advent of phase rotation techniques such as the frequently used SLM, there are many derivative approaches developed based on SLM that jointly modify amplitudes of signal candidates. Those works add non-constant amplitudes on original symbols, the purpose of which is addressed from different aspects such as to minimize PAPR or to eliminate SI to overcome the shortcomings of the SLM.

In paper [58] the researcher proposed a phase rotation method for PAPR reduction that includes minimizing the peak value of OFDM signal amplitudes over the signs, and alternating amplitudes of each subcarrier by implementing two individual optimization algorithm. This method contributes to the further reduction on PAPR than the conventional SLM technique, however, this method still requires SI, additionally increased signal power and computational complexity.

Paper [38] describes PIAT, a derivative of SLM that applies a power coefficients vector after the IFFT blocks to reshape OFDM signal amplitudes. It then selects the lowest one for transmission along with SI.

Paper [41] proposes a new SLM technique. Prior to the IFFTs, it utilizes a set of sequences that either enlarges magnitude with extension factor D or rotates the phase with

π on original symbols. At the receiver, through calculating the Hamming distance to estimate position of factor D, it allows to retrieve information about amplitude and phase modification sequence which have been selected to help recovering the original data symbols, without transmitting any SI. The expression of sequence which jointly modifies the phase and amplitude is defined as

$$\underline{P}^{u} = \left(De^{j\pi} \right)^{p_u}, \;\; p_u \in \{0,1\}, \tag{4.5}$$

where *D* is the magnitude extension factor.

In this dissertation, this method is used for performance comparisons in Chapter 5 and briefly named as *A-SLM*, indicating amplitude modified SLM method. This method reduces the risk of unrecoverable data error caused by sending SI, but relatively increases transmitted signal power accordingly.

4.2.2 Partial Transmit Sequences

The partial transmit sequence (PTS) technique performs the PAPR reduction using as many IFFT operations as the number of subblocks, and exhaustively searching the optimal combinations of subblocks and phase rotation coefficients throughout a given phase set. Figure 4.3 displays the block diagram of the partial transmit sequence (PTS) technique for PAPR reduction.

The PTS technique partitions an input data vector of *N* symbols into *V* subblocks as follows

$$X = \left[X^{0}, X^{1}, ..., X^{V-1} \right]^{T}, \tag{4.6}$$

where X^v is one of the subblocks that are consecutively located and evenly partitioned. It is unlike the SLM method in which each duplicated signal is multiplied with a phase sequence vector, each subblock in the PTS is rotated with a phase coefficient independently by multiplying a corresponding complex factor called weighting coefficient $b^v = \exp\left(j\psi^v\right)$. The V shifting phases of these weighing coefficients are selected inside a given phase set consisted of W complex weighting coefficients as $\psi^v = \left\{\psi^w \in [0, 2\pi), w = 0,1,...,W-1\right\},\ v = 0,1,...,V-1$.

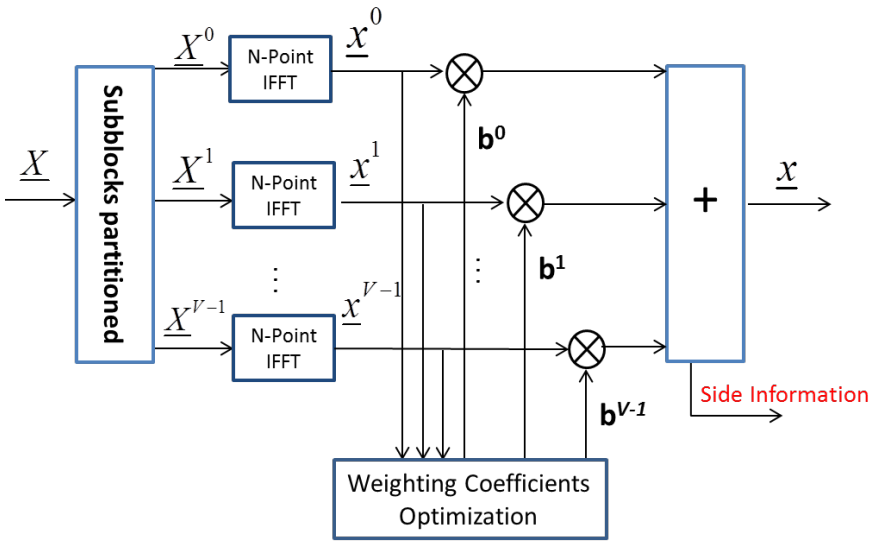

Figure 4.3 Block diagram of partial transmit sequence (PTS) technique for PAPR reduction.

PTS is methodologically similar to the SLM except a set of V subblocks partitioned from the original data symbol vector are first multiplexed by the IFFTs individually. Then, the transmit signal with the minimum PAPR is generated by optimally combining these sub-blocks with phase shifting coefficients selected from W complex weighting coefficients set [25], [26].

Therefore, a set of IFFT operators is required for all candidate OFDM frames at the transmitter both in the SLM and PTS methods. Moreover, for the purpose of recovering original data symbols by recognition on the corresponding phase shifting sequence/coefficients, side information per OFDM frame is requested to be sent to the receiver in an error-free fashion. In particular, the exhaustive search for minimum PAPR leads to an exponential increase in the computational complexity which is proportional to the number of subblocks [59].

4.2.3 Walsh-Hadamard Transform

In the Walsh-Hadamard transform precoded OFDM (WHT-OFDM) system [43], the original symbol vector is transformed by WHT before passing through the IFFT block at the transmitter without increasing power. The block diagram is shown in Figure 4.4.

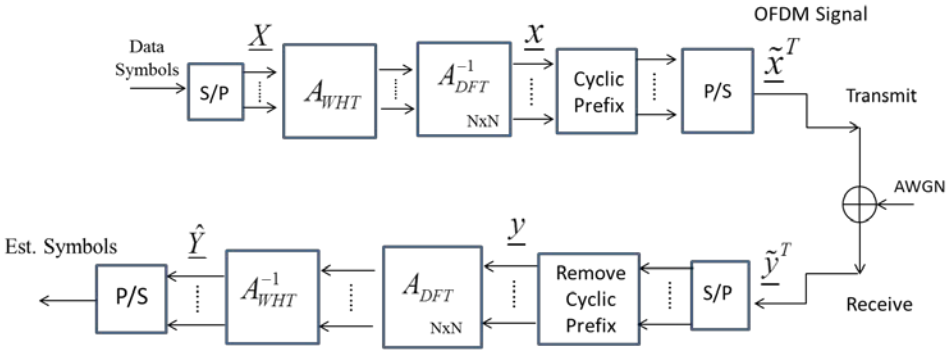

Figure 4.4 Block diagram of Walsh-Hadamard transform precoded OFDM (WHT-OFDM) for PAPR reduction.

The Walsh-Hadamard transform has been introduced in Section 2.1. As aforementioned, the constant modulus orthogonal transform matrix does not alternate the total power of original data symbols. Therefore, the WHT method improves PAPR without any power increase and side information requirement in a low-complexity system, and

accordingly does not induce BER degradation. But its PAPR performance is inferior to SLM, A-SLM and PTS methods. The WHT-OFDM based PAPR reduction method is used for PAPR and BER performance comparison in Chapter 5.

CHAPTER 5

SYMBOL ALPHABET MODIFIER MATRIX

The trade-off in the introduced PAPR reduction methods is existed such as increased average power, degraded BER performance, and added computational complexity. A new PAPR reduction scheme is proposed in this chapter that implements a pre-designed *symbol alphabet modifier matrix* (SAM) to change the amplitude and phase values of the original data symbols prior to the IFFT operation of an OFDM system at the transmitter. The receiver can recover original data symbols by employing the corresponding inverse SAM after FFT without BER degradation.

The proposed method is a marked departure from the existing ones and offers a simple framework devised to be independent of original data symbols, elegantly formulates the PAPR reduction problem, and significantly outperforms PTS, SLM and WHT-OFDM for the communication scenarios considered in the chapter.

5.1 Design Objective

Herein a low complexity PAPR reduction method is introduced for the OFDM systems that jointly modifies phase and amplitude of the original symbol alphabet such as *M*-PSK and *M*-QAM modulations.

The difference between peak power and mean power that is expressed as $\left| \max_{n=0,1,\ldots,N-1} |x(n)|^2 - E\left[|x(n)|^2 \right] \right|$ should be minimized by any PAPR reduction method. Conceptually, in the ideal case, all components of the OFDM frame vector $\underline{x}$ which have the same amplitude can limit the PAPR to be **1 (0 dB)** and the power difference to be zero.

The design motivation for a proper symbol alphabet modifier is first to find such an $N \times N$ matrix C^{-1} instead of the inverse discrete Fourier transform (DFT) matrix A_{DFT}^{-1} that can map a symbol vector into an OFDM frame with constant amplitude components. Here superscript '-1' is used to indicate the inverse matrix such that all matrices designed at the transmitter are identical to the denotation of the inverse DFT matrix A_{DFT}^{-1} and also implied to be invertible, this conversely at the receiver. Hence, it is necessary to define the design constraints such that the matrix C^{-1} must be invertible at the receiver and factorable to the A_{DFT}^{-1} matrix which served as the frequency selective orthogonal multiplexer.

5.2 Design Procedure

The design steps are explained as follows:

a) First, define an $N \times N$ transform matrix C^{-1} consists of complex value elements as

$$C^{-1} = \left[c_n(k) \right] = \left[\alpha_{k,n} \cdot e^{j\varphi_n(k)} \right] \quad k, n = 0,1,...,N-1, \tag{5.1}$$

where the amplitude of matrix elements is $\alpha_{k,n} \in \mathbb{R}^+$, k and n denote for column and row indices of a matrix. Then, the OFDM frame in time domain is expressed as

$$x(n) = \sum_{k=0}^{N-1} c_n(k)\,\mathrm{X}(k) \qquad n = 0,1,...,N-1. \tag{5.2}$$

Again, the $X(k)$ is the k^{th} component in the M-PSK or M-QAM modulated data symbol alphabet vector $\underline{X} = [X(0), X(1),..., X(N-1)]^T$ in frequency domain. The amplitude of each component is calculated as

$$\left|x(n)\right| = \left|\sum_{k=0}^{N-1} c_n(k)\,\mathrm{X}(k)\right|. \tag{5.3}$$

Then, by inspection, forcing the equality of two arbitrary components in an OFDM frame as the following relationship

$$\begin{aligned} &\left|x(m)\right| = \left|e^{j\triangle\phi_{m,n}}\right| \cdot \left|x(m)\right| = \left|x(n)\right| \\ &x(n) = \sum_{k=0}^{N-1} c_m(k) e^{j\triangle\phi_{m,n}} \cdot X(k) \\ &n, m = 0,1,\ldots,N-1, n \neq m, \end{aligned} \tag{5.4}$$

where $\Delta\phi_{m,n}$ denotes the phase difference between the n^{th} and m^{th} components of the OFDM frame vector. From (5.4), an intuitive design of the n^{th} and m^{th} rows of matrix C^{-1} is given as follows

$$\begin{aligned} &c_n(k) = c_m(k) \cdot e^{j\triangle\phi_{m,n}} \qquad n \neq m,\ n, m, k = 0,1,\ldots,N-1 \\ &\Rightarrow \alpha_{k,n} \cdot e^{j\varphi_n(k)} = \alpha_{k,m} \cdot e^{j\varphi_m(k)} \cdot e^{j\Delta\phi_{m,n}} \\ &\Rightarrow \alpha_{k,n} = \alpha_{k,m} = \alpha_k, \quad \varphi_n(k) = \varphi_m(k) + \Delta\phi_{m,n} = \varphi(k) + \Delta\phi_n, \end{aligned} \tag{5.5}$$

where $\triangle\phi_n = \triangle\phi_{0,n}$, $\varphi(k) = \varphi_0(k)$ is the phase of the k^{th} element in the first row ($m = 0$) of the matrix C^{-1}.

b) Now, express C^{-1} as

$$C^{-1} = \left[c_n(k)\right] = \left[\alpha_k \cdot e^{j(\varphi(k)+\Delta\phi_n)}\right] \quad k, n = 0,1,\ldots,N-1 \tag{5.6}$$

where $\alpha_k \in \mathbb{R}^+$, $\varphi(k)$ and $\triangle\phi_n \in [0, 2\pi)$, $\triangle\phi_0 = \triangle\phi_{0,0} = 0$. Note that the matrix C^{-1} is a constant modulus matrix when $\alpha_k = 1$.

Such a transform matrix can always map or multiplex any original symbol vector into a constant modulus OFDM frame vector. However, this matrix is not invertible because the rank of such a matrix is 1 and the data symbol vector cannot be recovered at the receiver [60]. In order to make the matrix C^{-1} invertible, the diagonal elements of the matrix C^{-1} is adjusted to be constant but non-unit amplitude α, and the remaining elements to have another amplitude β such that it has the full rank *N*. Moreover, if all rows or columns of such a matrix are permutated, it still maintains the full rank property [61]. The PAPR of the OFDM frame vector also remains the same. Accordingly, the modified matrix C^{-1} can be designed in different permutation forms of the initial adjusted matrix that provides many possible transformation sets as presented in following part c).

After modification on the amplitudes of matrix C^{-1}, those data symbols generated from the *M*-PSK can be transformed into a constant modulus OFDM frame when setting β to zero. Although the *M*-QAM modified symbols cannot be multiplexed into a constant modulus OFDM frame, a significant improvement on the PAPR compared to the PTS, SLM and WHT will be shown in Section 5.5.

c) Define a given permutation $\tilde{N}$ with *N* elements that $\tilde{N} : \{0,1,...,N-1\} \rightarrow \{0,1,...,N-1\}$ [62]. For example, when $N = 4$, the permutated order can be $\tilde{N} : \{2,0,3,1\}$. The modified matrix $\tilde{C}^{-1}$ that is invertible can be employed as follows

$$\tilde{c}_n(k) = \begin{cases} \alpha \cdot e^{j(\varphi(k)+\Delta\phi_n)} & k = \tilde{N}(n) \\ \beta \cdot e^{j(\varphi(k)+\Delta\phi_n)} & k \neq \tilde{N}(n) \end{cases} \tag{5.7}$$
$$= \alpha^{I_{\tilde{N}(n)}(k)} \cdot \beta^{1-I_{\tilde{N}(n)}(k)} \cdot e^{j(\varphi(k)+\Delta\phi_n)}, \quad k,n = 0,1,...,N-1$$

where $\alpha \in (0,\infty), \beta \in [0,\infty), \alpha > \beta,\ \varphi(k)$ and $\triangle\phi_n \in [0,2\pi),\ \triangle\phi_0 = 0$,

$\varphi(k) = \varphi(0) + A_k\pi$ for simplicity and $A_k \in \mathbb{Z}$.

$\mathrm{I}_n(k)$ is called *Indicator Function* [63], having the value 1 for element *k* equals to element *n* and the value 0 for element *k* different than set *n*, which is defined as

$$\mathrm{I}_n(k) = \begin{cases} 1 & \text{if } k = n \\ 0 & \text{if } k \neq n \end{cases}. \tag{5.8}$$

To express the modified matrix $\tilde{C}^{-1}$ more intuitively, let vector $\underline{\eta}^T = \left[e^{j\varphi(k)}\right]_{k=0}^{N-1}$, vector $\underline{\psi}^T = \left[e^{j\Delta\phi_n}\right]_{n=0}^{N-1}$, matrix $\Sigma_1 = diag(\underline{\eta}), \Sigma_2 = diag(\underline{\psi})$ and a real matrix displayed as

$$\Gamma = \begin{pmatrix} \alpha & & \beta \\ & \ddots & \\ \beta & & \alpha \end{pmatrix}_{N\times N}, \tag{5.9}$$

with its arbitrarily permutated columns (or rows) as

$$\Gamma = \begin{pmatrix} \beta & \cdots & \alpha & \cdots & \beta \\ \beta & \cdots & \cdots & \beta & \alpha \\ \beta & \alpha & \cdots & \cdots & \beta \\ \beta & \cdots & \cdots & \alpha & \beta \\ \alpha & \beta & \cdots & \cdots & \beta \end{pmatrix}_{N\times N}. \tag{5.10}$$

Then, the modified matrix is expressed as $\tilde{C}^{-1} = \Sigma_1 \Gamma \Sigma_2$.

Some possible cases are invoked to build various matrices $\tilde{C}^{-1}$ by assigning different amplitude and phase values to the elements of the matrix, which will be discussed in detail in Section 5.3.

d) Now, $\tilde{C}^{-1}$ should be factorized into an inverse DFT matrix A_{DFT}^{-1} and a matrix B^{-1} since the OFDM system needs to be built up with utilization of the IFFT operator. The invertible matrix B^{-1} is called *Symbol Alphabet Modifier matrix* (SAM) and is expressed in the matrix form as

$$\begin{aligned} \tilde{C}^{-1} &= A_{DFT}^{-1} \cdot B^{-1} \qquad \tilde{C} \cdot \tilde{C}^{-1} = I \\ B^{-1} &= A_{DFT} \cdot \tilde{C}^{-1} \qquad B \cdot B^{-1} = I, \end{aligned} \tag{5.11}$$

where B^{-1} is derived from (5.7) and (5.11) as

$$\begin{aligned} B^{-1} &= \left[\tilde{b}_k(n) \right]_{SAM} \qquad k,n = 0,1,...,N-1 \\ \tilde{b}_k(n) &= \sum_{l=0}^{N-1} e^{-j\frac{2\pi kl}{N}} \cdot \tilde{c}_n(l) = \sum_{l=0}^{N-1} \alpha^{I_{\tilde{N}(n)}(l)} \cdot \beta^{1-I_{\tilde{N}(n)}(l)} \cdot e^{j\left(\varphi(l)+\Delta\phi_n-\frac{2\pi kl}{N}\right)}. \end{aligned} \tag{5.12}$$

One can normalize the power of the modified symbols close to the original ones before the IFFT operator by dividing with a normalization factor of Frobenius matrix norm as $\left\| B^{-1} \right\|_F \Big/ \sqrt{N}$ [64]. The SAM matrix B^{-1} is rewritten as

$$B^{-1} = \left[\frac{\tilde{b}_k(n)}{\sqrt{\sum_{k=0}^{N-1}\sum_{n=0}^{N-1} \left| \tilde{b}_k(n) \right|^2 \Big/ N}} \right]_{SAM} \qquad k,n = 0,1,...,N-1. \tag{5.13}$$

The Figure 5.1 displays the block diagram of the OFDM system employed with the proposed SAM method over additive white Gaussian noise (AWGN) and multipath fading channels.

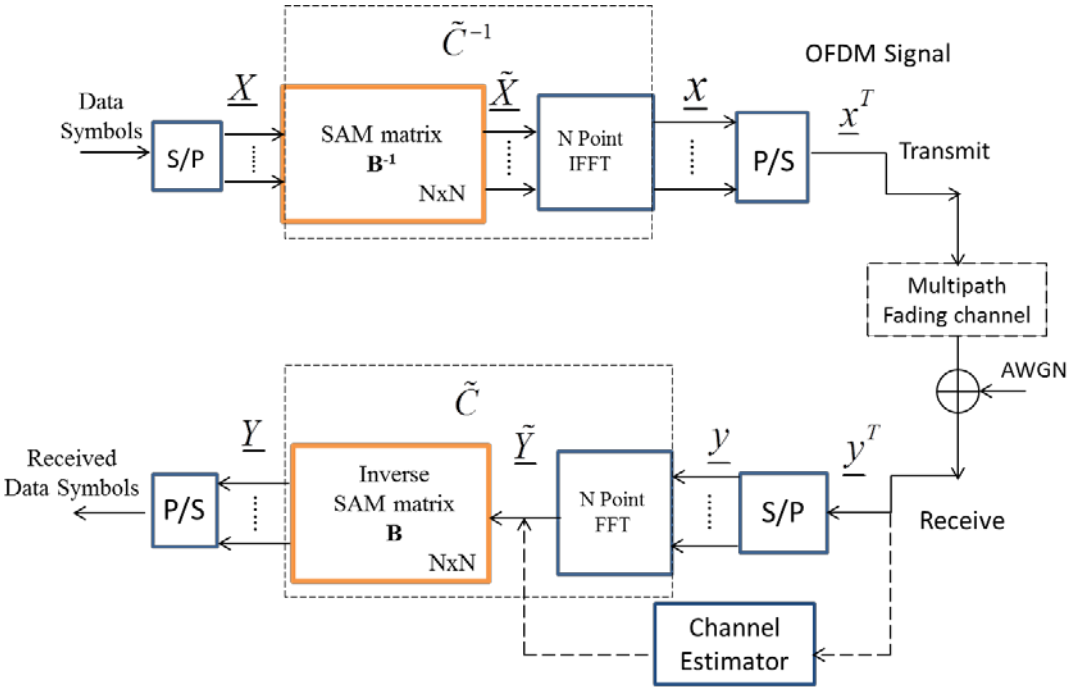

Figure 5.1 Block diagram of the OFDM system with the proposed PAPR reduction method.

5.3 Frameworks of the Symbol Alphabet Modifier Matrix

In this section, some possible cases are pursued and investigated based on function (5.7).

5.3.1 Invertible SAM Matrix (Case 1)

Case 1: in this case, the amplitudes α, β are positive real numbers and $\alpha > \beta$, the matrix $\tilde{C}^{-1}$ can be normalized to $\tilde{c}_n(k) = \tilde{\alpha}^{I_{\tilde{N}(n)}(k)} \cdot e^{j(\varphi(k)+\Delta\phi_n)}$, here $\tilde{\alpha} = \alpha/\beta$. For readability, use α instead of $\tilde{\alpha}$, and has

$$\tilde{c}_n(k) = \begin{cases} \alpha \cdot e^{j(\varphi(k)+\Delta\phi_n)} & k = \tilde{N}(n),\ k,n = 0,1,...,N-1 \\ e^{j(\varphi(k)+\Delta\phi_n)} & k \neq \tilde{N}(n) \end{cases}. \quad (5.14)$$

In case 1, the SAM matrix B^{-1} is not a constant modulus matrix such that it modifies the amplitude as well as average power of the original data symbols. But the difference between the modified power and the original one is subtle and trivial, where the numerical results tabulated in Table 5.1 has validated. The theoretical derivation on the predictable dynamic range of signal amplitudes in Appendix A also confirmed this.

5.3.2 Orthogonal SAM Matrix (Case 2)

Case 2: where β is zero, the matrix $\tilde{C}^{-1}$ becomes a constant modulus diagonal matrix and the value of parameter α can be normalized to 1 as

$$\tilde{c}_n(k) = \begin{cases} e^{j(\varphi(k)+\Delta\phi_n)} & k = \tilde{N}(n),\ k,n = 0,1,...,N-1 \\ 0 & k \neq \tilde{N}(n) \end{cases}. \quad (5.15)$$

As a result, according to the function (5.11), it can be obtained in case 2 that the SAM matrix B^{-1} is an orthogonal matrix which modifies the amplitude of original data symbols without alternating total signal power.

***Remark**: It is observed that when B^{-1} is a constant modulus diagonal matrix, it represents one of the phase sequences in the ordinary SLM technique. Moreover, the matrix factorization in (5.11) leads to the Generalized DFT (GDFT) framework reported in [3]as follows*

$$A_{GDFT}^{-1} = A_{DFT}^{-1} \cdot G^{-1} = e^{j\frac{2\pi}{N}kn} \cdot g_{k,n} e^{j\theta_{k,n}} \qquad k = n = 0,1,...,N-1. \quad (5.16)$$

where $g_{k,n}$ and $\theta_{k,n}$ denote for the amplitude and phase of the k^{th} column and n^{th} row element in G matrix.

As introduced in Section 4.2.1, each phase sequence in the SLM is a vector $\underline{B}^u = [\mathrm{b}_0^u, \mathrm{b}_1^u, ..., \mathrm{b}_{N-1}^u]$, $u = 0,1,...,U-1$, $\mathrm{b}_k^u = e^{j\psi_k^u}$ and phase ψ_k^u is uniformly selected in range of $[0, 2\pi)$. Each phase sequence multiplied with inverse DFT matrix resulting in the new composition matrix expressed as

$$A_{SLM}^u = A_{DFT}^{-1} \cdot diag\left(\underline{B}^u\right) = e^{j\frac{2\pi}{N}kn} \cdot \mathrm{b}_k^u = e^{j\left(\frac{2\pi}{N}kn + \psi_k^u\right)} \quad k,n = 0,1,...,N-1, \qquad (5.17)$$

which reveals the fact that the SLM is a special solution of the proposed SAM framework.

In Appendix A, the dynamic range of the amplitudes of OFDM frame applying SAM method in case 1 and case 2 is discussed. It verifies that, due to the axial symmetry in the *M*-point symbol alphabet constellation, the amplitude value of the OFDM component yields no more than $(M+2)(M-1)/2$ possible values for *M*-QAM and only one value for *M*-PSK with an increase of α times value, which can be normalized to be 1 as shown in (5.15). Accordingly, the boundary of the peak power can be estimated, and the PAPR performance is varied over the value of α in case 1 while case 2 is an orthogonal (unitary) matrix with normalized $\alpha = 1$.

Compared to the amplitude values of the OFDM frame modified by the inverse DFT (original OFDM frame) that have many more possibilities, the amplitude variations of the proposed SAM method with case 1 and case 2 in the time domain are shown in Figure 5.2 (α=100 is taken for case 1 and α=1 in case 2). It is seen that amplitudes of OFDM

frame modified by the proposed SAM method are more concentrated and less fluctuating in the time domain. Hence, the PAPR performance is significantly improved.

In Section 5.3.3 and 5.3.4, the extension frameworks of the previous matrix $\tilde{C}^{-1}$ shown as case 3 and case 4 are discussed.

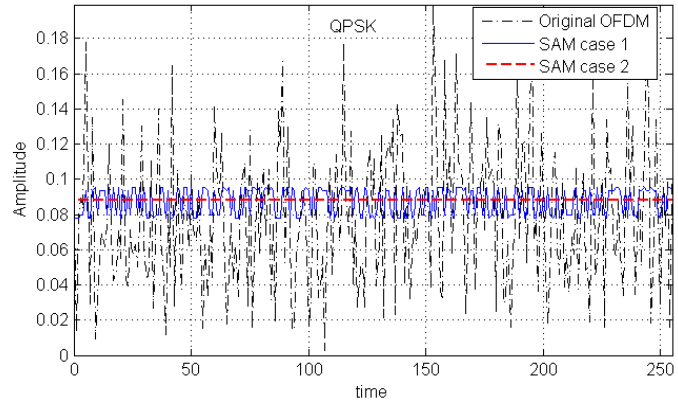

(a)

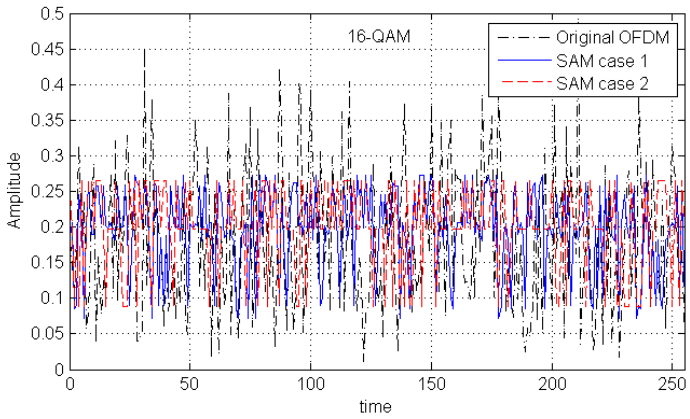

(b)

Figure 5.2 Amplitudes of the OFDM frame with case 1 and case 2 for a) QPSK and b) 16-QAM.

5.3.3 Extension on Orthogonal SAM Matrix (Case 3)

In the above, the proposed framework of matrix $\tilde{C}^{-1}$ with two cases is designed for PAPR reduction by reducing the dynamic range of the time domain signals. The matrix format

expression is provided by the product function $\tilde{C}^{-1} = \Sigma_1 \Gamma \Sigma_2$ as shown in (5.9) or its arbitrarily permutated columns (or rows) as in (5.10). In case 2, the matrix $\tilde{C}^{-1}$ becomes an unitary (diagonal) matrix expressed as

$$\tilde{C}^{-1} = \begin{pmatrix} e^{j(\varphi(0)+\Delta\phi_0)} & & 0 \\ & \ddots & \\ 0 & & e^{j(\varphi(N-1)+\Delta\phi_{N-1})} \end{pmatrix}_{N\times N}, \tag{5.18}$$

and thus the corresponding SAM matrix is an orthogonal matrix due to the unitary property of discrete Fourier transform and accordingly has $B \cdot B^H = I$. It is proved in function (5.16), (5.17) and (5.20) that when $\beta = 0$, the PAPR performance of OFDM frames has been enhanced to reach an optimum reduction performance and is independent of the original data symbols.

In case 1, although the matrix $\tilde{C}^{-1}$ and SAM matrix B^{-1} are invertible and provide similarity to orthogonal transform activities with respect to the PAPR and BER performance when parameter α approaching a large value, they are not orthogonal matrices in fact. Only when α takes a value such as 100 or larger (verified in Appendix A), the matrix $\tilde{C}^{-1}$ and SAM are getting close to the activities that orthogonal matrix achieved, and also reflected on PAPR and BER performance which are numerically validated in Section 5.4.

In case 2 (β=0，α=1), the matrix $\tilde{C}^{-1}$ becomes an unitary matrix (diagonal matrix), without permutation the sequence of each row in matrix Γ is the cyclic shifted version of the previous row. Regarding the orthogonality of SAM matrix derived from

matrix $\tilde{C}^{-1}$ in (5.12), the received signal can be retrieved without BER degradation compared to the original OFDM signal which is theoretically verified in Appendix A.

Instead of using the complex sequence with amplitudes of $[\alpha, \beta, ..., \beta]$ as the basis one in the previous design, a new sequence $\underline{S}$ denoted as basis sequence, along with its cyclic shifted ones, build up a new size of $N \times N$ matrix $\tilde{C}^{-1}$ namely case 3. The constrain of matrix $\tilde{C}^{-1}$ should be a unitary matrix that always promise no BER degradation at the receiver.

The new matrix $\tilde{C}^{-1}$ in case 3 is expressed as

$$\tilde{C}^{-1} = \begin{pmatrix} \underline{S}^{T} \\ \underline{S}^{(1)T} \\ \vdots \\ \underline{S}^{(N-1)T} \end{pmatrix}_{N \times N} . \tag{5.19}$$

Here, the superscript (n), $n = 0,1,...,N-1$ indicates the n times right cyclic shift of the basis sequence $\underline{S}^{T}$.

Hence, for the purpose of eliminating unwanted BER degradation, this basis sequence denoted as $\underline{S} = [s_0, s_1, ..., s_{N-1}]^{T}$ is required to be a complex value sequence having perfect periodic auto-correlation property that is described as

$$R_S(m) = \sum_{k=0}^{N-1} S[k] S^{*}[(k+m) \bmod N] = E_S \delta(m \bmod N), \tag{5.20}$$

where m as the cyclically shifted delays is an integer and E_S is the peak energy in a single period of auto-correlation.

The auto-correlation of matrix $\tilde{C}^{-1}$ reveals the reason of requesting perfect periodic auto-correlation sequences, which is proved by the derivation as

$$\begin{aligned}\tilde{C}^{-1}\cdot\left(\tilde{C}^{-1}\right)^{H} &= \begin{pmatrix} \underline{S}^{T} \\ \underline{S}^{(1)T} \\ \vdots \\ \underline{S}^{(\mathrm{N}-1)T} \end{pmatrix}\begin{pmatrix} \underline{S}^{*} & \underline{S}^{(1)*} & \cdots & \underline{S}^{(\mathrm{N}-1)*} \end{pmatrix} \\ &= \begin{pmatrix} \underline{S}^{T}\underline{S}^{*} & \underline{S}^{T}\underline{S}^{(1)*} & \cdots & \underline{S}^{T}\underline{S}^{(\mathrm{N}-1)*} \\ \vdots & \underline{S}^{(1)T}\underline{S}^{(1)*} & & \vdots \\ & & \ddots & \\ \underline{S}^{T}\underline{S}^{(\mathrm{N}-1)*} & \cdots & & \underline{S}^{(\mathrm{N}-1)T}\underline{S}^{(\mathrm{N}-1)*} \end{pmatrix} \\ &= \left|\underline{S}^{T}\underline{S}^{*}\right|\begin{pmatrix} 1 & & 0 \\ & \ddots & \\ 0 & & 1 \end{pmatrix}.\end{aligned} \tag{5.21}$$

This satisfies the constraint of $\tilde{C}^{-1}\cdot\left(\tilde{C}^{-1}\right)^{H} = I$ after normalization and thereby $B^{-1}\cdot\left(B^{-1}\right)^{H} = I$.

By looking at the previous design of case 2, it can be found that when strengthening a few data symbol values by parameter α and weakening others by parameter β, as the output of the matrix $\tilde{C}^{-1}$, the OFDM signal's power will be reduced into a smaller dynamic range compared to the original OFDM signal's. When $\beta = 0$, the emphasis brings an optimal effect on PAPR reduction.

Therefore, case 3 as an extension of case 1 for matrix $\tilde{C}^{-1}$ is proposed to have the basis sequence which is defined as

$$\underline{S} = \left[\underbrace{s_0,0,\ldots}_{N/L},\underbrace{s_1,0,\ldots}_{N/L},\ldots,\underbrace{s_{L-1},0,\ldots}_{N/L}\right]^{T}, \tag{5.22}$$

and the n^{th} row is generated as the n times shifted version of (5.22), for instance, taking $n = N/L$ is shown to have

$$\underline{S}^{(N/L)} = \left[\underbrace{s_{L-1}, 0, ...}_{N/L}, \underbrace{s_0, 0, ...}_{N/L}, \underbrace{s_1, 0, ...}_{N/L}, ..., \underbrace{s_{L-2}, 0, ...}_{N/L} \right]^T, \tag{5.23}$$

where the non-zero tapping sequence $\underline{\hat{S}} = \left[s_0, s_1, ..., s_{L-1} \right]^T$ is a perfect periodic auto-correlation sequence such as Zadoff-Chu sequence given by [65]

$$\hat{S}[k] = \exp\left(\frac{j\pi}{N} k(k+1) \right), \qquad k = 0,1,...,L-1. \tag{5.24}$$

Herein, utilizing the Zadoff-Chu sequence of length 4 (L=4) as the non-zero tapping sequence $\underline{\hat{S}}$ to populate the basis sequence in (5.22). The PAPR performance is simulated for this design in case 3 and provided in Section 5.5, with QPSK and 16-QAM modulated respectively. From the observation of PAPR and BER performance obtained in case 3, it can be seen that although the promise of no BER degradation is achieved, an acquisition of competitive PAPR reduction needs to be further pursued for the *M*-QAM modulated data symbols.

5.3.4 Extension on Orthogonal SAM Matrix Case 3 (Case 4)

Nonetheless, the aforementioned constant amplitude polynomial sequences having perfect periodic auto-correlation property such as Zadoff-Chu sequence cannot bring an

outstanding peak power reduction for OFDM signals without any emphasis impacted on the data symbols.

In view of this, to achieve a better PAPR performance in the new extensive framework of $\tilde{C}^{-1}$, the improved design for the basis sequence is proposed to have two non-zero components as

$$\underline{S} = \left[s_0, \underbrace{0,\ldots,}_{N/2-1} s_1, \underbrace{0,\ldots}_{N/2-1} \right]^T, \tag{5.25}$$

where s_0 and s_1 are non-constant amplitude complex values used to emphasize the data symbols.

Intuitively, such sequence should promise the perfect periodic auto-correlation as shown in (5.19), thus, it can be derived as

$$\begin{cases} s_0 s_1^* + s_1 s_0^* = 0 \\ s_0 s_0^* + s_1 s_1^* \neq 0 \end{cases} \tag{5.26}$$

Let $s_0 = \alpha e^{j\theta_0}$ and $s_1 = \beta e^{j\theta_1}$, where α and $\beta \in \mathbb{R}^+$. Substitute them into the function (5.25), it yields

$$\begin{aligned} s_0 s_1^* + s_1 s_0^* &= \alpha\beta \cdot \left[\exp\left(j\left(\theta_0 - \theta_1\right)\right) + \exp\left(-j\left(\theta_0 - \theta_1\right)\right)\right] \\ &= \alpha\beta \cdot \cos\left(\theta_0 - \theta_1\right) = 0 \end{aligned} \tag{5.27}$$

and also has

$$s_0 s_0^* + s_1 s_1^* = \alpha^2 + \beta^2 \neq 0. \tag{5.28}$$

As a result, it should have $\theta_0 - \theta_1 = \{\pm\pi/2, \pm 3\pi/2\}$, θ_0 and $\theta_1 \in [0, 2\pi)$.

Due to the existing zero tapping inside the basis sequence, the periodic auto-correlation $R_S(m)$ in (5.20) is always zero when the correlation shifting delay at the moment of $(m \bmod N/2) \neq 0$ for this case. Therefore, the *n* times right shifted sequence $\underline{S}^{(n)}$ denoted as the n^{th} row of the new matrix $\tilde{C}^{-1}$ could be relaxed and not necessarily the cyclic shifted version of the first row that is the basis function $\underline{S}$ expressed in function (5.25), while $n = 1, 2, ..., N/2 - 1$.

For $n = 0, 1, ..., N/2 - 1$, propose the n^{th} row sequence of the new matrix $\tilde{C}^{-1}$ to be

$$\underline{S}^{\langle n \rangle} = \left[\underbrace{0, ..., 0}_{n}, \underbrace{s_0^{\langle n \rangle}, 0, ..., 0}_{N/2}, \underbrace{s_1^{\langle n \rangle}, 0, ..., 0}_{N/2-n} \right]^T, \tag{5.29}$$

For $n = N/2, ..., N - 1$, the n^{th} row sequence becomes the flipping version of the sequence at the row index of $n - N/2$ as

$$\underline{S}^{\langle n \rangle} = \left[\underbrace{0, ..., 0}_{n-N/2}, \underbrace{s_1^{\langle n-N/2 \rangle}, 0, ..., 0}_{N/2}, \underbrace{s_0^{\langle n-N/2 \rangle}, 0, ..., 0}_{N-n} \right]^T, \tag{5.30}$$

where $s_0^{\langle n \rangle} = \alpha^{\langle n \rangle} e^{j\theta_0^{\langle n \rangle}}$ and $s_1^{\langle n \rangle} = \beta^{\langle n \rangle} e^{j\theta_1^{\langle n \rangle}}$, $\alpha^{\langle n \rangle}$ and $\beta^{\langle n \rangle} \in \mathbb{R}^+$.

Here, the phase difference between the two elements remains as $\theta_0^{\langle n \rangle} - \theta_1^{\langle n \rangle} = \{\pm\pi/2, \pm 3\pi/2\}$, $\theta_0^{\langle n \rangle}$ and $\theta_1^{\langle n \rangle} \in [0, 2\pi)$. Note that instead of using (n) to

indicate the n^{th} cyclic shifting on the basis sequence, $\langle n \rangle$ is used to denote the n^{th} distinct sequence in the matrix $\tilde{C}^{-1}$.

Besides, in order to achieve the design motivation and objective, for the purpose to simplify the expression of the new matrix, let $\alpha^{\langle n \rangle} = \alpha$, $\beta^{\langle n \rangle} = \beta$. As a result, such new matrix $\tilde{C}^{-1}$ is a unitary matrix as well as its column permutated matrices. After normalization for SAM matrix to avoid unnecessary power increasing, the components of the sequence are changed as

$$\begin{aligned} s_0^{\langle n \rangle} &= \frac{\alpha}{\sqrt{\alpha^2 + \beta^2}} \cdot \exp\left(j\theta_0^{\langle n \rangle} \right), \\ s_1^{\langle n \rangle} &= \frac{\beta}{\sqrt{\alpha^2 + \beta^2}} \cdot \exp\left(j\theta_1^{\langle n \rangle} \right). \end{aligned} \tag{5.31}$$

Let $\beta = 1$, $\hat{\alpha} = \alpha / \beta$, for continuity, still use α instead of $\hat{\alpha}$. To instantiate this design, the matrix $\tilde{C}^{-1}$ of size 8×8 is shown below

$$\tilde{C}^{-1} = \begin{bmatrix} s_0 & 0 & 0 & 0 & s_1 & 0 & 0 & 0 \\ 0 & s_0^{\langle 1 \rangle} & 0 & 0 & 0 & s_1^{\langle 1 \rangle} & 0 & 0 \\ 0 & 0 & s_0^{\langle 2 \rangle} & 0 & 0 & 0 & s_1^{\langle 2 \rangle} & 0 \\ 0 & 0 & 0 & s_0^{\langle 3 \rangle} & 0 & 0 & 0 & s_1^{\langle 3 \rangle} \\ s_1 & 0 & 0 & 0 & s_0 & 0 & 0 & 0 \\ 0 & s_1^{\langle 1 \rangle} & 0 & 0 & 0 & s_0^{\langle 1 \rangle} & 0 & 0 \\ 0 & 0 & s_1^{\langle 2 \rangle} & 0 & 0 & 0 & s_0^{\langle 2 \rangle} & 0 \\ 0 & 0 & 0 & s_1^{\langle 3 \rangle} & 0 & 0 & 0 & s_0^{\langle 3 \rangle} \end{bmatrix}_{8 \times 8} \tag{5.32}$$

The amplitudes of the OFDM frame populated by the inverse DFT (original OFDM frame) and the proposed SAM method with case 3 and case 4 in the time domain are shown

in Figure 5.3 a and b ($\alpha = 100$ is chosen for the case 4 as explained in Appendix B). It is seen that amplitudes of OFDM frame modified by the proposed SAM method in case 4 is more concentrated and less fluctuating in the time domain. Although it is not satisfied on minimizing the difference between mean and peak amplitudes (same to peak power) in case 3, but it still lessens the peak amplitude value than original OFDM signal. According to this, the PAPR performance is significantly improved in case 4 with $\alpha = 100$. The numerical simulation and comparisons in Section 5.5 show the PAPR performance by employing SAM in case 3 and case 4 when α takes different values.

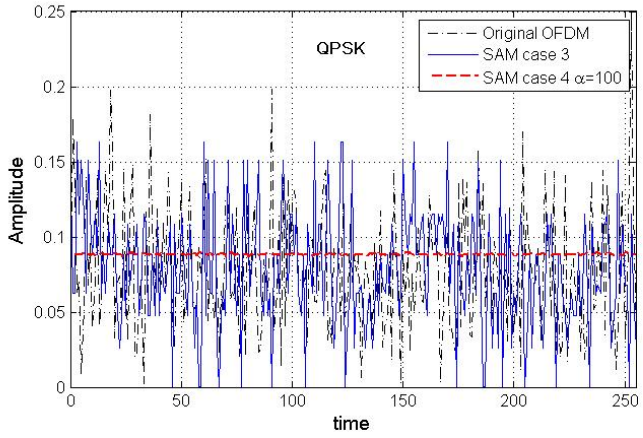

(a)

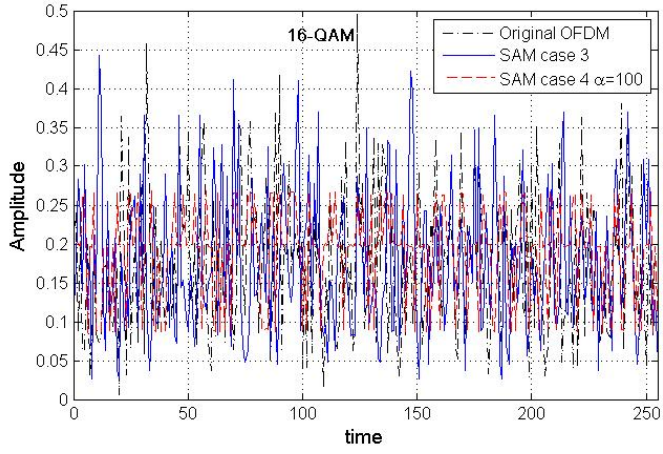

(b)

Figure 5.3 Amplitudes of the OFDM frame with case 3 and case 4 for a) QPSK and b) 16-QAM.

The dynamic range of the peak power for OFDM signals which employ the proposed case 4 with *M*-PSK or *M*-QAM modulated can be estimated in a constrained boundary. It is stated and evaluated in Appendix B that the performance of PAPR is dependent on the value of parameter α.

5.4 PAPR and BER Performance Estimation

The performance of the PAPR reduction technique can be quantified in terms of achieving an expected bit error rate (BER) at a given signal-to-noise ratio (SNR). With the main focus of improving PAPR performance, it is sometimes compensated at the expense of increased BER, such as SLM and PTS techniques require side information to be transmitted, along with the aforementioned amplitude modified SLM (A-SLM) method which increases signal power. Below, it is verified that the proposed method approaches PAPR reduction without BER degradation when the SAM matrix B^{-1} is an orthogonal matrix presented in case 2, case 3 and case 4. In case 1, the evaluating results given in Figures 5.7 and 5.8 have shown that when parameter α is at a large enough value such as 100, the BER performance of it is approximately the same to the other three orthogonal cases.

The estimation of received data symbols adapting SAM method after IFFT and inverse SAM matrix *B* is obtained in frequency domain as

$$Y = B \cdot B^{-1} X + B \cdot W_0 = I \cdot X + B \cdot W_0, \tag{5.33}$$

where W_0 denotes the complex additive white Gaussian noise (AWGN) vector with zero mean and variance $\sigma_{w_0}^2$.

At the receiver, after passing through the inverse SAM matrix (the orthogonal ones in case 2 ,case 3 and case 4), $E\left[\left(W_0^H B^H\right)\left(BW_0\right)\right] = E\left[W_0^H W_0\right] = \sigma_{w_0}^2 I$, where $[\cdot]^H$ denotes the Hermitian operator, I is the identity matrix, the noise vector BW_0 has the same mean and variance as AWGN vector W_0. Accordingly, the proposed SAM matrix won't cause BER degradation in AWGN channel, which can be shown in Section 5.5.

5.5 PAPR and BER Performance Comparisons

The performance simulation results are presented in this section. Table 5.1 tabulates the average power fluctuation (in dB) of the proposed SAM in four cases (superscripts such as 1 and 2 denote for case 1 and case 2 respectively), WHT, PTS, SLM, A-SLM methods for QPSK and 16-QAM with $N = 64$ subcarriers. In the A-SLM, the number of amplitude modified symbols in each sequence is uniformly distributed in the interval [0, Smax] where parameters Smax = 6, and D = 2.4 with QPSK and D = 4.4 with 16-QAM were used as suggested in [41]. As seen from the Table 5.1, in case 1, when the value of α is larger, the power fluctuation of OFDM frame is approaching zero. In case 2, case 3 and case 4, the SAM matrix B^{-1} is orthogonal, accordingly without inducing additional power or any sacrifice on signal distortion, the power of the original symbols will not be changed with power normalization as in (5.13).

The OFDM system simulations are performed for all four cases (choose $\alpha = 100$ in case 1 and case 4, $\alpha = 1$ in case 2, $L = 4$ in case 3) of the proposed SAM method with $\varphi(0) \in [0, 2\pi)$ as selected randomly, and choosing $\varphi(l) = \varphi(0) + l\pi$, $\Delta\phi_n = n\pi/4$ in function (5.12). Besides, $\theta_0^{\langle n \rangle} - \theta_1^{\langle n \rangle} = \{\pm\pi/2, \pm 3\pi/2\}$, $\theta_0^{\langle n \rangle}$ or $\theta_1^{\langle n \rangle}$ is stochastically chosen in

the range of $[0,2\pi)$ for function (5.30) in case 4, where the permutation $\tilde{N}$ is arbitrarily generated for all cases.

Table 5.1 Average Power Variations of SAM in Four Cases, PTS, SLM, A-SLM and WHT for QPSK and 16-QAM with N = 64

N = 64	**Power varied**	**Power varied**
WHT	0	0
PTS	0	0
SLM	0	0
A-SLM	2.5	4.2
SAM[1] α =10^3	<10^{-3}	<10^{-3}
SAM[1] α =100	0.03	0.1
SAM[2]	0	0
SAM[3]	0	0
SAM[4]	0	0

The complexities of various methods considered in the dissertation are tabulated in Table 5.2. In PTS and SLM techniques, *U* and *V* IFFT operations are required. Besides, side information bits are used along with OFDM signal transmission to the receiver. On the other hand, the proposed SAM and WHT need only one pair of FFT/IFFT operations and no SI bits are required at the receiver.

In the calculation of $\tilde{C}^{-1}$ in case 1 and case 2, vector $\underline{\eta}^T = \left[e^{j\varphi(k)}\right]_{k=0}^{N-1}$ and vector $\underline{\psi}^T = \left[e^{j\Delta\phi_n}\right]_{n=0}^{N-1}$ totally require 2*N* multiplications and zero additions. When $\varphi(l) = \Delta\phi_n = 0$, zero multiplications and additions are needed. Matrix Γ requires *N* multiplications and $2N-1$ additions for Case 1 (where $\beta = 1$), and zero multiplications and additions for Case 2 (where $\alpha = 1$, $\beta = 0$). In the approach of case 3, when the matrix $\tilde{C}^{-1}$ consists of only one basis sequence along with its all cyclically shifted versions, there are *LN* multiplications and *N*(*L*-1) additions required, where $L = 4$ is taken to implement

Zadoff-Chu sequence for the following simulation on PAPR and BER performance comparisons. As proposed in case 4, 2N multiplications and N additions are needed. In addition, the Discrete Fourier transform of the modified matrix $\tilde{C}^{-1}$ yields the SAM matrix as shown in (5.11). Therefore, adapting IFFT operation in (5.11) to obtain the SAM matrix requires $N\log_2(N)/2$ multiplications and $N\log_2(N)$ additions.

Table 5.2 System Complexity of SAM, PTS, SLM and WHT Methods for OFDM System

N=64	**SI (Bit)**	**# of IFFTs**	**# of Complex Multip.**	**# of Complex Add.**
Original	No	1	$N\log_2(N)/2$	$N\log_2(N)$
WHT	No	1	$N\log_2(N)/2+N^2$	$N\log_2(N)+N(N-1)$
PTS	Yes	V	$VN\log_2(N)/2+VW^{V-1}$	$VN\log_2(N)$
SLM	Yes	U	$NU\log_2(N)/2+UN$	$UN\log_2(N)$
SAM[1]	No	1	$N\log_2(N)+N$	$2N\log_2(N)+2N-1$
SAM[2]	No	1	$N\log_2(N)$	$2N\log_2(N)$
SAM[3]	No	1	$N\log_2(N)+LN$	$2N\log_2(N)+N(L-1)$
SAM[4]	No	1	$N\log_2(N)+2N$	$2N\log_2(N)+N$

The SAM method has raised the computational complexity to original OFDM systems, but apparently, the proposed method has much lower computational complexity than the other methods where the comparisons on multiplication and addition complexities are plotted in Figure 5.4. While there is only 3 bits SI chosen for comparative study in Figure 5.4, the computational cost of SLM and PTS methods grow fast as the number of candidates/sub-blocks increases. It should be noted that, in the following BER performance comparisons, it is assumed an error free situation of SI transmission in SLM

and PTS methods such that no data loss caused by SI will be considered. But in practical term, this is inevitable unless additional cost are paid to cover it.

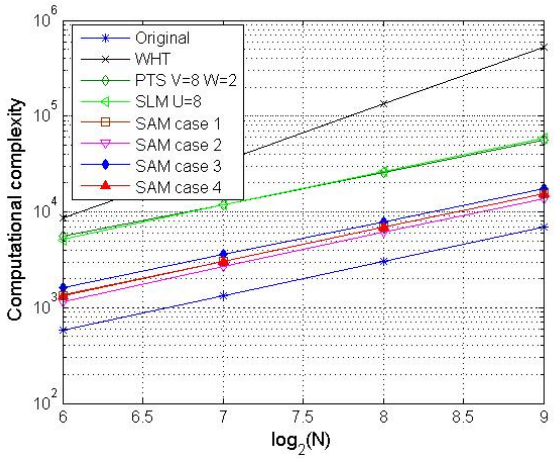

Figure 5.4 Computational complexity comparison of the proposed SAM in four cases, WHT-OFDM, PTS, and ordinary SLM methods.

Figure 5.5 displays the PAPR performance of the proposed SAM method in case 1 and case 2, along with several values of parameter α comparable for case 1 with QPSK, 16-QAM and 64-QAM. Similarly, Figure 5.6 is plotted for case 3 and case 4.

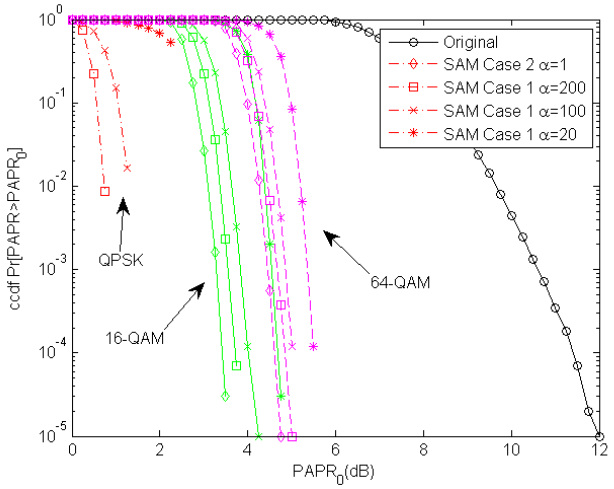

Figure 5.5 PAPR performance of the proposed SAM in case 1 and case 2 for QPSK, 16-QAM, 64-QAM and N=128 in the OFDM system.

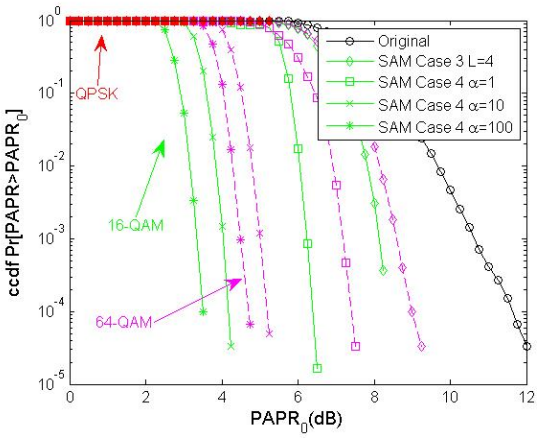

Figure 5.6 PAPR performance of the proposed SAM in case 3 and case 4 for QPSK, 16-QAM, 64-QAM and N=128 in the OFDM system.

Figures 5.7 and 5.8 illustrate the CCDFs performance (aforementioned in Section 4.1) of the proposed SAM in case 1 and case 2, WHT-OFDM, PTS, ordinary SLM and A-SLM methods. For QPSK and subcarriers $N = 128$, the OFDM signals in the SLM and A-SLM have candidates $U = 8$ and 64, Smax =12, D=2.4, while subblocks $V = 8$ and 32, phase coefficients $W = 2$ are used for PTS. Also $U = 8$ and 128, Smax=25, D=4.4, $V = 8$ and 64, $W = 2$ for 16-QAM and signal length $N = 256$, respectively. The CCDFs are simulated by randomly generating 100,000 OFDM frames for each method.

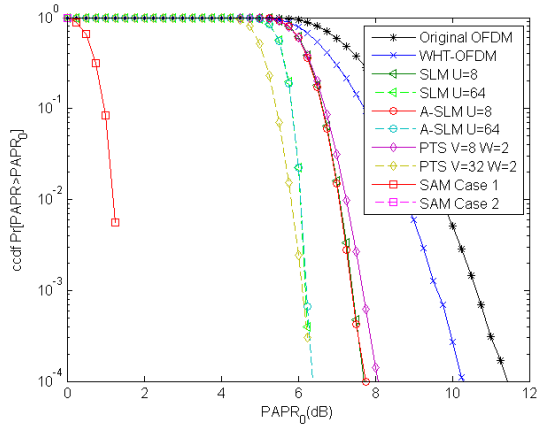

Figure 5.7 PAPR performance of the proposed SAM in case 1 and case 2, WHT-OFDM, PTS, ordinary SLM, and A-SLM methods for QPSK and N=128.

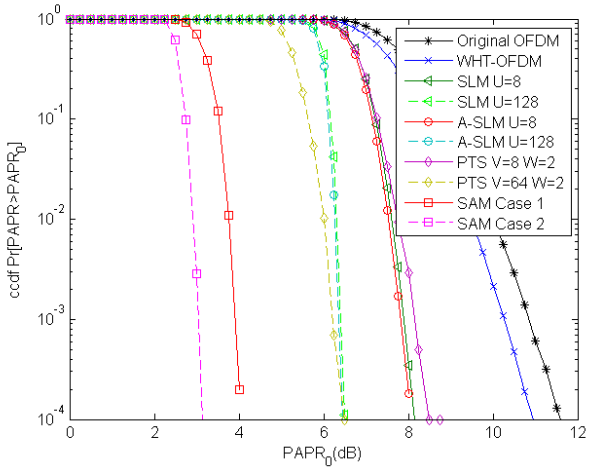

Figure 5.8 PAPR performance of the proposed SAM in case 1 and case 2, WHT-OFDM, PTS, ordinary SLM, and A-SLM methods for 16-QAM and N=256.

Figures 5.9 and 5.10 display the BER performance comparisons over the AWGN channel and the multipath fading channel with utilization of high power amplifier (HPA). The multipath fading channel is assumed to be a three-path Rayleigh fading channel with equal power. The HPA is modeled as Rapp's solid state power amplifier (SSPA) given as [66], the output signal of the SSPA is defined as

$$r_{out} = \frac{r_{in}}{\left(1 + r_{in}^{2p}\right)^{1/2p}}, \tag{5.34}$$

where r_{in} and r_{out} denote the amplitude of input and output signals, and $p = 2$ is chosen to approximate a practical power amplifier as suggested in [66].

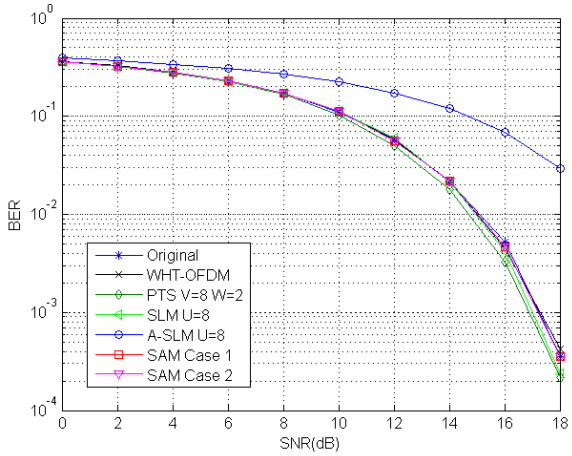

Figure 5.9 BER performance comparisons of the proposed SAM in case 1 and case 2, WHT-OFDM, PTS, ordinary SLM, and A-SLM methods for 16-QAM and N=256 over AWGN channel.

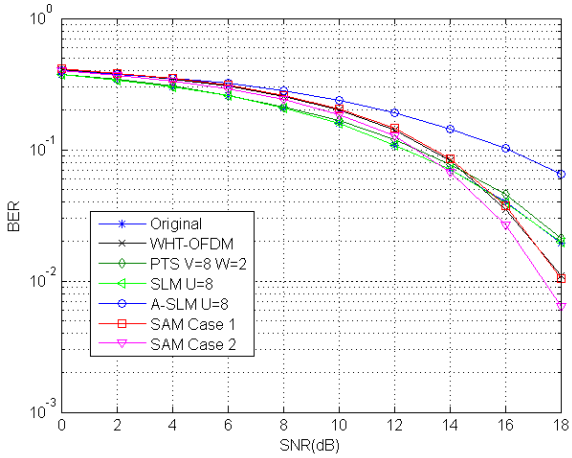

Figure 5.10 BER performance comparisons of the proposed SAM in case 1 and case 2, WHT-OFDM, PTS, ordinary SLM, and A-SLM methods for 16-QAM and N=256 over multipath fading channel.

The PAPR performance of the proposed SAM method in case 3 and case 4 are also compared and presented for QPSK and 16-QAM with the signal length $N = 256$, implementing Zadoff-Chu sequence with $L = 4$ in case 3, and $\alpha = \{1, 10, 100\}$ in case 4 as illustrated in Figures 5.11 and 5.12.

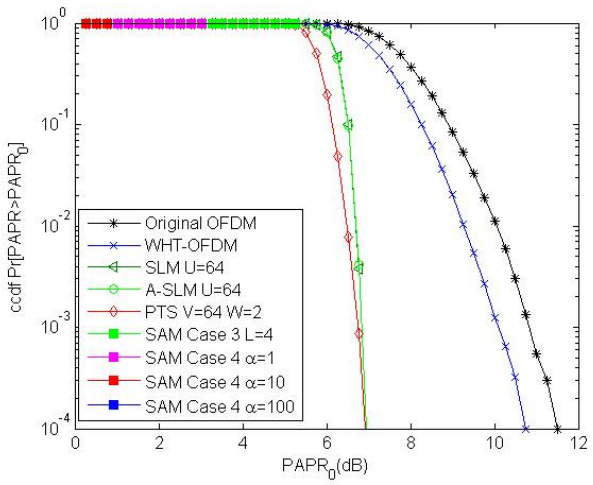

Figure 5.11 PAPR performance of the proposed SAM in case 3 using ZC sequence and case 4 (with different α values), WHT-OFDM, PTS, ordinary SLM, and A-SLM methods when L=4, N=256, for QPSK.

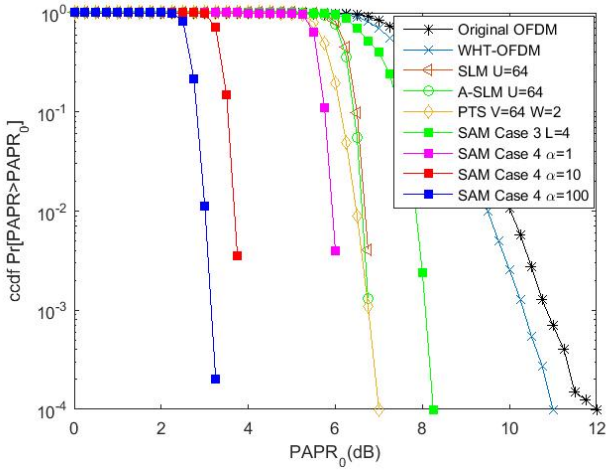

Figure 5.12 PAPR performance of the proposed SAM in case 3 using ZC sequence and case 4 (with different α values), WHT-OFDM, PTS, ordinary SLM, and A-SLM methods when L=4, N=256, for 16-QAM.

It can be seen that when α gets larger in case 4, the PAPR provides better performance, especially in *M*-PSK modulated data symbols, the considerable improvements on PAPR over SLM and PTS are achieved even when $\alpha = 1$. When $\alpha = 100$ in case 4 with QPSK, the PAPR is approaching the value of 1 (0dB), which has been reached in case 2 and was shown in Figure 5.7. The design of sequence in case 4

provides a better PAPR reduction than the same framework in case 3 using Zadoff-Chu sequence. Also, the design of SAM method in case 4 outperforms PTS, SLM and WHT methods both in QPSK and 16-QAM when $\alpha > 10$ in Figures 5.11 and 5.12.

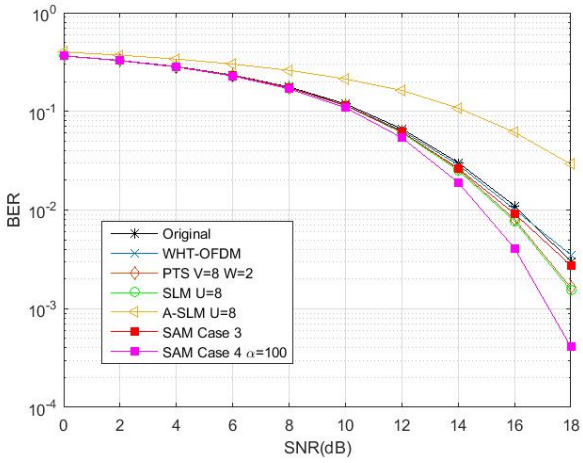

Figure 5.13 BER performance comparisons of the proposed SAM in case 3 using ZC sequence, case 4 when $\alpha = 100$, WHT-OFDM, PTS, ordinary SLM, and A-SLM methods for 16-QAM and N=256 over AWGN channel.

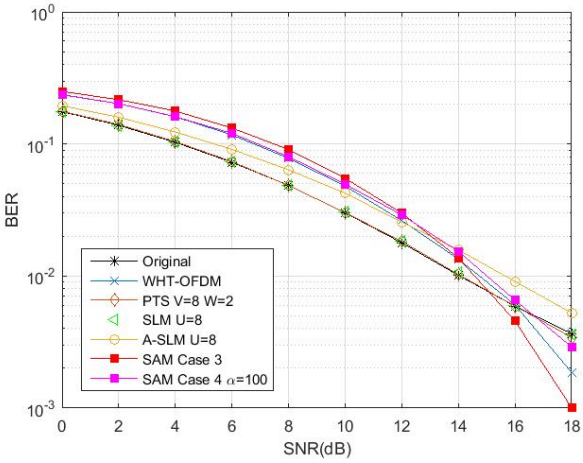

Figure 5.14 BER performance comparisons of the proposed SAM in case 3 using ZC sequence, case 4 when $\alpha = 100$, WHT-OFDM, PTS, ordinary SLM, and A-SLM methods for 16-QAM and N=256 over multipath fading channel.

Similarly, the BER performance comparisons with SAM method employed in case 3 and case 4 over the AWGN channel and the multipath fading channel with SSPA customized in (5.34) are also displayed in Figures 5.13 and 5.14. The BER performance of the SAM method has validated the design motivation for case 3 and case 4.

These performance results confirm that the proposed SAM method significantly outperforms PTS, SLM and WHT techniques in PAPR reduction. Case 2 as the ultimate form of case 1, at the CCDF rate of 10^{-3} as a threshold, yields a PAPR gain of 0 dB for QPSK and 3 dB for 16-QAM. Case 1 yields 0.8 dB for QPSK and 3.9 dB for 16-QAM, whereas the original OFDM signal is 10.2 dB and 11.1dB respectively. In Case 4, as discussed in Appendix B, where α=100 is chosen for comparison, displays considerable improvement on PAPR reduction. Due to the orthogonality, case 2, 3 and 4 retain the original OFDM signal's BER theoretically, while case 1 with a large α also approached the same performance as shown in Figures 5.9 and 5.10.

The Table 5.3 shows the comparisons between all proposed cases in SAM method and other popular techniques introduced with respect to the PAPR gain of CCDF at a given rate of 10^{-3}, where α=100 in case 1 and case 4, $L = 4$ in case 3 with Zadoff-Chu sequence.

It can be seen from the Table 5.3 that the proposed method in case 2 and case 4 prominently reduced the PAPR for various constellation scenarios. Meanwhile, case 1 and case 3 also powerfully enhanced the PAPR performance over other popularly implemented methods for OFDM systems.

Table 5.3 PAPR Gain (dB) at the CCDF Rate of 10^{-3} of SAM in Four Cases, PTS, SLM, A-SLM and WHT for QPSK and 16-QAM Modulations with $N = 256$

N=256	**QPSK**	**16-QAM**
Original	10.9	11.1
WHT	10.0	10.5
PTS	6.8	7.0
SLM	6.7	6.9
A-SLM	6.8	7.0
SAM^1	1.2	3.9
SAM^2	0	3.0
SAM^3	5.2	8.8
SAM^4	0.1	3.0

A significant PAPR improvement is achieved by the proposed SAM method, especially in case 2 and case 4, it presents a better performance than case 1 and case 3, also outperforms all other methods for PAPR reduction without BER degradation. Hence, the OFDM system with the proposed SAM method reduces power consumption of HPA and avoids BER degradation caused by in-band interference. It should be noted that PTS and SLM methods require SI bits to be transmitted without any error tolerance such that the receiver can recover the original data without failure. On the other hand, it should be highlighted that the SAM method does not need to reserve bits for the transmission of the SI, resulting in the increase of the data rate, and is simple to implement with respect to the lower computational complexity as well as only one pair FFT/IFFT operations.

CHAPTER 6

PAPR REDUCTION FOR STBC MIMO-OFDM SYSTEMS

In this chapter, an implementation of the proposed symbol alphabet modifier matrix (SAM) that elegantly formulates PAPR reduction problem in STBC MIMO-OFDM will be described. Moreover, the proposed method significantly improves PAPR without BER degradation that permits much lower computational complexity and implementation cost compared to the SLM based systems for the application scenarios also presented in this chapter.

6.1 STBC MIMO-OFDM Systems

MIMO wireless communication systems offer great interest due to its potential for different sources of diversity and spatial multiplexing, which can be properly exploited by a proper coding and transmission scheme. Multiple antennas and space time codes can be used to obtain spatial diversity. Frequency diversity can be utilized in an orthogonal frequency division multiple access system. However, the MIMO-OFDM systems still suffer from high PAPR as the main drawback caused by OFDM signals.

6.1.1 Alamouti MIMO-OFDM Systems

The maximum diversity can be realized using the space-time block codes proposed by Alamouti by providing a simple transmit diversity scheme in a flat fading multiple-input multiple(MIMO) channel [67]. The OFDM methodology converts a wide band frequency to multiple narrow bands which almost have flat frequency in an efficiency use, so one can use MIMO with OFDM to transmit data in wide band frequencies achieving high

efficiency and low bit error rate. Space time or space frequency along with OFDM can utilize the orthogonal transmission by Alamouti MIMO systems.

Here, the Alamouti MIMO-OFDM system is considered to adopt space-time block coding (STBC) method with two transmit antennas and one or more receive antennas. First, the incoming data bit stream is mapped to a sequence of symbols $X(k), k = 0,1,...,N-1$ from a predefined Symbol Alphabet (SA) that populate the symbol vector $\underline{X} = [X_0, X_1, ..., X_{N-1}]^T$, where N is the number of subcarriers and $[\cdot]^T$ denotes vector/matrix transpose operator. At time period t_0, one input data symbol vector $\underline{X}_0$ is multiplexed by IDFT and transmitted from the first antenna TX_0. Similarly, another data symbol vector $\underline{X}_1$ is also inverse transformed by IDFT and transmitted from the second antenna TX_1. During the next signal period $t_0 + T$, data symbol vector $-\underline{X}_1^*$ is transmitted by the first antenna TX_0 and vector $\underline{X}_0^*$ by the second antenna TX_1, where T is OFDM frame duration. The two data symbol vectors inverse transformed and transmitted from the two antennas are expressed as

$$\begin{pmatrix} X_{TX_0} \\ X_{TX_1} \end{pmatrix} = \begin{pmatrix} \underline{X}_{2m} & -\underline{X}_{2m+1}^* \\ \underline{X}_{2m+1} & \underline{X}_{2m}^* \end{pmatrix} \qquad m = 0,1,... \tag{6.1}$$

where $(\cdot)^*$ denotes a complex conjugate operator and m denotes m^{th} set transmitted STBC symbol vectors during every time period T.

The OFDM frame transmitted by the i^{th} antenna, $\underline{x}_{TX_i} = [x_i(0), x_i(1), ..., x_i(N-1)]^T$, is obtained through IDFT as [67]

$$x_{TX_i}(n) = \frac{1}{\sqrt{N}} \sum_{k=0}^{N-1} X_{TX_i}(k) e^{j\frac{2\pi kn}{N}}, \quad n = 0,1,...,N\text{-}1 \;\; i = 0,1. \tag{6.2}$$

PAPR of the signal fluctuation in an OFDM frame at each antenna is defined by

$$PAPR_i = \frac{\max_{n=0,1,...,N-1} \left| x_{TX_i}(n) \right|^2}{E\left[\left| x_{TX_i} \right|^2 \right]} \qquad i = 0,1, \tag{6.3}$$

where $E[\cdot]$ denotes the expectation operator. Therefore, the overall PAPR of the STBC MIMO-OFDM system is given as

$$\text{PAPR} = \max_{i=0,1} \{ PAPR_i \}. \tag{6.4}$$

Here, i is the index number of the transmitting antenna.

By conjugating the signal transmitted from the second antenna, at one of the receivers, the received signals at the time slots of t and $t+T$, after demodulation to the frequency domain through FFT, are written as

$$\begin{aligned} Y_0 &= H_0 X_{2m} + H_1 X_{2m+1} + W_0 \\ Y_1 &= -H_0 X^*_{2m+1} + H_1 X^*_{2m} + W_1, \end{aligned} \tag{6.5}$$

where W denotes complex additive white Gaussian noise (AWGN), and H represents the multipath fading channels between the transmitted antennas and the received antenna with subscript ‘0’ and ‘1’ indicating from antenna TX_0 and TX_1, respectively.

Rewritten in the matrix form, (6.5) is given as

$$\begin{bmatrix} Y_0 \\ Y_1^* \end{bmatrix} = \begin{bmatrix} H_0 & H_1 \\ H_1^* & -H_0^* \end{bmatrix} \begin{bmatrix} X_{2m} \\ X_{2m+1} \end{bmatrix} + \begin{bmatrix} W_0 \\ W_1^* \end{bmatrix}. \tag{6.6}$$

Assuming that the channels' responses are perfectly estimated at the receiver, the output of the space-time decoder is derived from (6.6) to be

$$\begin{bmatrix} \hat{X}_{2m} \\ \hat{X}_{2m+1}^* \end{bmatrix} = \begin{bmatrix} H_0 & H_1 \\ H_1^* & -H_0^* \end{bmatrix}^{-1} \begin{bmatrix} Y_0 \\ Y_1^* \end{bmatrix}. \tag{6.7}$$

Therefore, the output signals of the space-time decoder can be separated by

$$\begin{aligned} \hat{X}_{2m} &= \frac{H_0^* Y_0 + H_1 Y_1^*}{|H_0|^2 + |H_1|^2}, \\ \hat{X}_{2m+1} &= \frac{H_1^* Y_0 - H_0 Y_1^*}{|H_0|^2 + |H_1|^2}. \end{aligned} \tag{6.8}$$

This is the so called zero-forcing algorithm. Such methodology brings the advantage of reducing the complexity at receiver with the received signal copies at two time slots that can be benefited by utilizing the information redundancy.

6.1.2 SLM Employed Alamouti MIMO-OFDM Systems

The SLM is a probabilistic algorithm to reduce the possibility of high PAPR by first generating several OFDM frames (a library of frames) for the same symbol vector, and then selecting the one with the lowest PAPR prior to transmission. In the implementation in STBC MIMO-OFDM [68], [69], each one of duplicates of the original data symbol vector $\underline{X}$ in frequency domain is multiplied with phase shifting sequence (Phase Modifier)

$\underline{B}^u$ and goes through the IFFT of each, as shown in Figure 4.1. The U phase modifier vectors are described as

$$\underline{B}^u = \left\{ b^u(k) = e^{j\psi^u(k)}, k = 0,1,...,N-1 \right\} \quad u = 0,1,...,U-1. \tag{6.9}$$

where $\psi^u(k) \in [0, 2\pi)$. The modified symbol vector $\underline{X}^u$ at the u^{th} branch is generated as

$$X^u(k) = b^u(k) X(k) \qquad k = 0,1,...,N\text{-}1. \tag{6.10}$$

The modified OFDM frame set with the minimum PAPR is identified and transmitted, where the optimal phase shifting sequence is selected as

$$\hat{u}_i = \arg \min_{u=0,...,U-1} \left\{ PAPR_i^u \right\} \quad i = 0,1. \tag{6.11}$$

Then, two symbol vectors $\underline{X}_0^{\hat{u}_0}$ and $\underline{X}_1^{\hat{u}_1}$ are encoded by the Alamouti STBC to generate data symbol vectors in the next time period. These vectors are transformed into time domain with an IFFT operator. In general, $\log_2 U$ bits of side information per OFDM frame for each transmitter need to be sent to the receiver in an error-free fashion [68]. This procedure is depicted in Figure 6.1.

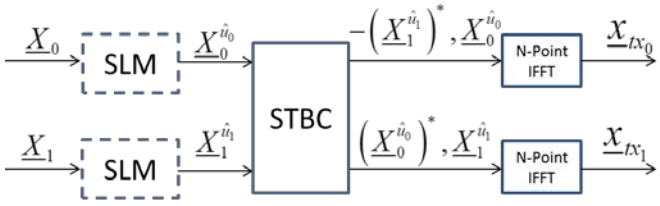

Figure 6.1 Block diagram of transmitters employed SLM technique for PAPR reduction in STBC MIMO-OFDM system.

6.2 Implementation of SAM Matrix in STBC MIMO-OFDM Systems

As addressed in Chapter 5, the proposed SAM is implemented in the STBC MIMO-OFDM system. The block diagram of the framework is illustrated in Figure 6.2. After the received signals are transformed by the forward Fourier transform block and inverse SAM matrix *B*, the estimation functions of them are gives as

$$\begin{aligned} \hat{X}_0 &= B\frac{H_0^* Y_0 + H_1 Y_1^*}{|H_0|^2 + |H_1|^2}, \\ \hat{X}_1 &= B\frac{H_1^* Y_0 - H_0 Y_1^*}{|H_0|^2 + |H_1|^2}. \end{aligned} \tag{6.12}$$

The amplitude values of the original OFDM frames that were modified by the inverse DFT have many possible outcomes. For comparison, the amplitudes of the MIMO-OFDM frame which employed the proposed SAM method with all four cases in the time domain are depicted in Figures 5.3 and 5.4. It can be seen that amplitudes of OFDM frame modified by the proposed SAM method are more concentrated and less fluctuating in the time domain, especially in case 2 and case 4 when constant amplitude modulation such as QPSK is applied, the amplitude of the OFDM signal is constant, providing the ideal PAPR property for the design motivation and objective. Accordingly, the PAPR of STBC MIMO-OFDM performance is significantly improved for every transmitter.

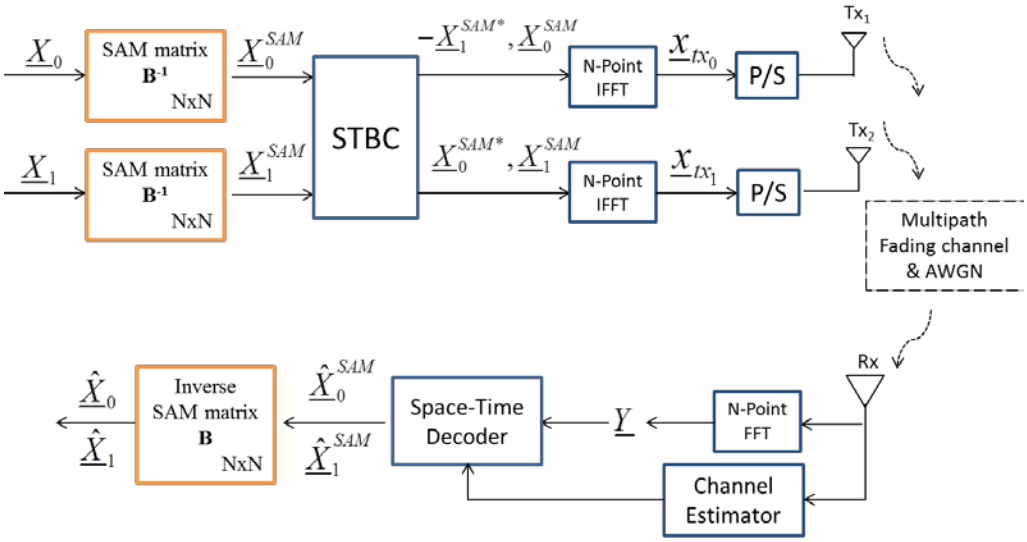

Figure 6.2 Block diagram of the proposed SAM technique employed in STBC MIMO-OFDM system.

6.3 PAPR and BER Performance

Table 6.1 tabulates the average power fluctuation (in dB) of the proposed SAM and SLM methods compared to original OFDM signals for QPSK when N=64, and 16-QAM when N=128. When the value of α is larger than 30, the power fluctuation of OFDM frame is almost zero. The power variation is negligible, less than 0.01dB, even when α gets smaller.

The PAPR and BER performance simulations are performed for all four cases ($\alpha = 100$ in case 1 and case 4) with QPSK and 16-QAM for the proposed SAM method with $\varphi_0(0) \in [0, 2\pi)$, $\varphi_0(n) = \varphi_0(0) + n\pi$, $\triangle\phi_m = n\pi/N$ as described in function (5.12), and $\theta_0^{\langle n \rangle} - \theta_1^{\langle n \rangle} = \{\pm\pi/2, \pm 3\pi/2\}$ in case 4 where $\theta_0^{(n)}$ or $\theta_1^{(n)}$ is randomly chosen in the range of $[0, 2\pi)$ for function (5.30). The permutation order with length $\tilde{N}$ is arbitrarily generated. The CCDFs are simulated by randomly generating 100,000 OFDM frames for each method.

The multipath fading channel of each is assumed to be a five-path Rayleigh fading channel with equal power and combined with complex AWGN channel.

Table 6.1 Average Power Variations of SLM and the Proposed SAM Methods for QPSK with N=64 and 16-QAM with N=128

	SI (Bit)/ Single Tx	**# of IFFTs/ Single Tx**	**Power Varied (QPSK) [dB]**	**Power Varied (16-QAM) [dB]**
SLM	3	8	0	0
SLM	6	64	0	0
SAM[1] $\alpha = 30$	0	1	$<10^{-5}$	$<10^{-5}$
SAM[1] $\alpha = 10$	0	1	0.001	0.002
SAM[2]	0	1	0	0
SAM[3]	0	1	0	0
SAM[4]	0	1	0	0

Figures 6.3 and 6.4 provide the CCDFs of the ordinary SLM method and the proposed SAM method with four cases ($\alpha = 100$ in case 1 and case 4, $\alpha = 1$ in case 2, $L = 4$ in case 3) in the four transmitters STBC MIMO-OFDM system. The corresponding BER performance at one of the receivers is displayed in Figure 6.5 with QPSK and 16-QAM modulated data symbol alphabets.

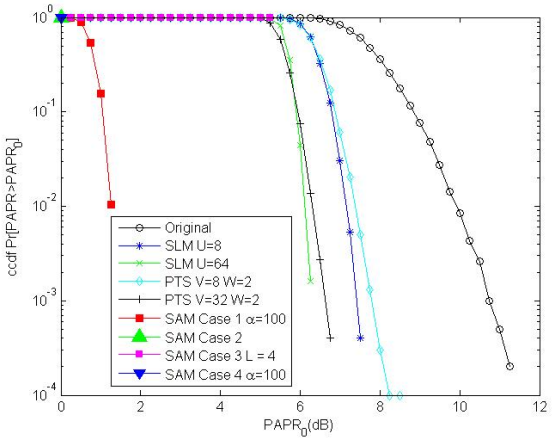

Figure 6.3 PAPR performance of the proposed SAM for various α and ordinary SLM (SI=3 and 6) for QPSK and N=128 in four transmitters STBC MIMO-OFDM system.

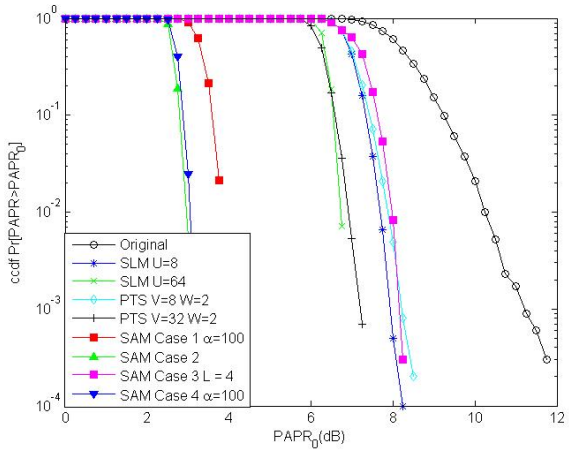

Figure 6.4 PAPR performance of the proposed SAM for various α and ordinary SLM (SI=3 and 6) for 16-QAM and N=256 in four transmitters STBC MIMO-OFDM system.

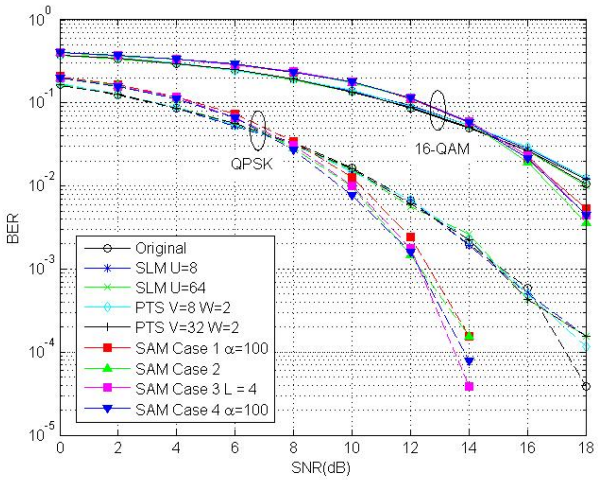

Figure 6.5 BER performance comparison of the proposed SAM in three cases, ordinary SLM and PTS (SI=3 and 6) over multipath fading channel for N=256 when QPSK and 16-QAM are employed respectively.

It is observed from Figures 6.3, 6.4 and 6.5 that the SAM method significantly outperforms the SLM method in PAPR reduction and also in BER. PAPR and BER performances are enhanced when the value of α is larger in case 1 and case 4. It is noted that the SLM method requires additional SI bits to be transmitted without any error tolerance. Theoretical analysis and simulation results show that the proposed method has the ability to provide outstanding PAPR reduction performance without BER degradation,

and also offers a low computational complexity without SI in the STBC MIMO-OFDM systems.

CHAPTER 7

CONCLUSIONS AND FUTURE WORK

The performance comparisons presented in the dissertation highlight the improvements offered by the Generalized Discrete Fourier Transform (GDFT) framework to design optimum waveforms for MIMO radar applications. GDFT is a marked departure from linear phase DFT, such that the entire phase space of constant modulus orthogonal bases is thoroughly exploited for the optimization of waveforms.

In addition to the orthogonality, the GDFT based waveforms are optimized for generating good auto- and cross-correlation properties for accurately estimating the moving target in radar systems. Moreover, it is shown that popular waveforms like MCPC and Oppermann types are special cases of the GDFT family. The examples of GDFT framework presented in the Chapter 3 provide design flexibility and can easily be extended for larger values of N. It is expected to see engineering implementations of GDFT based waveforms in the future with better performance.

Furthermore, the orthogonal Partial Matched Filter Bank offers a mechanism to sample the phase function of the received signal in a radar system where minimized correlations are desirable. Through combining it with the promising Generalized DFT in the proposed framework which samples the received waveform in the exponent part for Doppler estimation in radar, it is expected that the proposed approach may find its use in future radar systems.

In Chapter 5 of the dissertation, a new peak-to-average power ratio reduction method is proposed based on the phase and amplitude joint modifications in the symbol alphabet. The Symbol Alphabet Modifier matrix (SAM) technique provides a dramatic

reduction in PAPR performance and outperforms the WHT-OFDM, PTS and SLM based methods, especially for case 2 and case 4, which also form an orthogonal SAM matrix. Moreover, the proposed method has low-complexity framework to implement in OFDM systems and does not require any side information compared to other popular conventional PAPR reduction methods such as SLM and PTS.

The efficient PAPR reduction method SAM in the four proposed cases is implemented in the Space-Time Block Coding (STBC) MIMO-OFDM system. The method utilizes a predesigned symbol alphabet modification (SAM) matrix along with a single IFFT/FFT block pair in STBC MIMO-OFDM system. Here, the SAM technique provides dramatic reduction in PAPR performance over the ordinary SLM method. It also offers better BER than the latter. Moreover, its implementation and computational cost is significantly less than the popular SLM scheme.

As an extension of Discrete Fourier Transform (DFT) from the linear phase to non-linear phase, there are infinitely possible GDFT sets available in the phase space with constant or non-constant power and nonlinear phase functions. In comparison with several popular methods such as SLM and PTS mentioned in the dissertation, the proposed method is shown to be powerful in signal processing and communications. The GDFT framework offers its potential in correlation improvements, which can be largely exploited and employed in the MIMO radar system. One can design the optimal basis for the desired requirements and purposes by exploiting different types of G matrix which offers the large and pleasant freedom in the phase space. For future wireless communication systems, the combination of massive MIMO-OFDM with low complexity orthogonal block transforms will be one of the most expected candidates.

APPENDIX A

DYNAMIC RANGE OF OFDM SIGNAL AMPLITUDE IN CASE 1 AND CASE 2

Due to the properties imposed in the design of case 1 and case 2 of matrix $\tilde{C}^{-1}$, the amplitude of the components in an OFDM frame vector becomes

$$\begin{aligned}\left|x(n)\right| &= \left|e^{j\Delta\phi_n}\sum_{k=0}^{N-1}\alpha^{I_{\tilde{N}(n)}(k)}\cdot\beta^{1-I_{\tilde{N}(n)}(k)}\cdot e^{j\varphi(k)}\,\mathrm{X}(k)\right| \\ &= \left|\sum_{k=0}^{N-1}\alpha^{I_{\tilde{N}(n)}(k)}\cdot\beta^{1-I_{\tilde{N}(n)}(k)}\cdot e^{j\varphi(k)}\,\mathrm{X}(k)\right| \\ &= \begin{cases}\left|\sum_{k=0}^{N-1}\alpha^{I_{\tilde{N}(n)}(k)}\cdot e^{j\varphi(k)}\,\mathrm{X}(k)\right| & \beta=1 \\ \alpha\left|\mathrm{X}\left(\tilde{N}(n)\right)\right| & \beta=0\end{cases}.\end{aligned} \tag{A.1}$$

Suppose the arbitrary permutation on the rows of the matrix $\tilde{C}^{-1}$ has $\tilde{N}(n)=k_1, \tilde{N}(m)=k_2$, $k_1\neq k_2$ for the n^{th} and m^{th} components of the OFDM frame. Based on the theorem [70] $\left|\left|a\right|-\left|b\right|\right|\le\left|a-b\right|$, the amplitude difference between these two components is derived as

$$\begin{aligned}&\left|\left|x(n)\right|-\left|x(m)\right|\right| = \left|\left|S_1\right|-\left|S_2\right|\right| \le \left|S_1-S_2\right| \\ &= \left|\hat{S}_1-\hat{S}_2\right| = (\alpha-\beta)\left|e^{j\varphi(k_1)}\,\mathrm{X}(k_1)-e^{j\varphi(k_2)}\,\mathrm{X}(k_2)\right|,\end{aligned} \tag{A.2}$$

where

$$\begin{aligned}S_1 &= \alpha\cdot\mathrm{X}(k_1)e^{j\varphi(k_1)}+\sum_{\substack{k=0\\k\neq k_1}}^{N-1}\beta\cdot\mathrm{X}(k)e^{j\varphi(k)} \\ S_2 &= \alpha\cdot\mathrm{X}(k_2)e^{j\varphi(k_2)}+\sum_{\substack{k=0\\k\neq k_2}}^{N-1}\beta\cdot\mathrm{X}(k)e^{j\varphi(k)},\end{aligned} \tag{A.3}$$

and

$$\begin{aligned}\hat{S}_1 &= \alpha \cdot \mathrm{X}(k_1) e^{j\varphi(k_1)} + \beta \cdot \mathrm{X}(k_2) e^{j\varphi(k_2)} \\ \hat{S}_2 &= \alpha \cdot \mathrm{X}(k_2) e^{j\varphi(k_2)} + \beta \cdot \mathrm{X}(k_1) e^{j\varphi(k_1)}.\end{aligned} \tag{A.4}$$

The original symbol vector $\underline{X} = [X(0), X(1), ..., X(N-1)]^T$ is generated from an *M*-point symbol alphabet constellation such as *M*-PSK or *M*-QAM. Here, the phase function of the matrix is $\varphi(k) = \varphi(0) + A_k \pi$, such that $\left\{ e^{j\varphi(k)} X(k), k = 0,1,..., N-1 \right\} \in \{$*M*-PSK or *M*-QAM shifted by $\varphi(0)\}$. Therefore, $\left| e^{j\varphi(k_1)} \mathrm{X}(k_1) - e^{j\varphi(k_2)} \mathrm{X}(k_2) \right|$ has no more than $(M+2)(M-1)/2$ possible values in the symbol alphabet modulation. Note that when α is much larger than β, amplitudes of the components will be dominated by and approximately equivalent to the largest symbol in each summation function of (A.1). Accordingly, for case 1 (where β=1) the difference between the arbitrary two components will be

$$\begin{aligned}&\left\| x(n) \right| - \left| x(m) \right\| \approx \left\| \alpha \cdot e^{j\varphi(k_1)} \mathrm{X}(k_1) \right| - \left| \alpha \cdot e^{j\varphi(k_2)} \mathrm{X}(k_2) \right\| \\ &= \alpha \left\| \mathrm{X}(k_1) \right| - \left| \mathrm{X}(k_2) \right\|.\end{aligned} \tag{A.5}$$

As a result, this outcome is approximately the same as case 2 (β=0). After the normalization for case 2, the parameter $\alpha = 1$. The *M*-PSK modulated data symbol alphabets are constant amplitudes, such that any two data symbols have $\left| \mathrm{X}(k_1) \right| - \left| \mathrm{X}(k_2) \right| = 0$. For the *M*-QAM modulated data symbols, the maximum amplitude difference is given depending on the constellation map. In short, the dynamic range of the OFDM signal

amplitudes is straightforwardly pre-decided through calculating the largest amplitude difference in the data symbol vector $\underline{X}$.

From (A.5), it is also observed that the PAPR performance is independent of the phase vector $\underline{\psi}$ in matrix $\tilde{C}^{-1}$, and also independent of the phase vector $\underline{\eta}$ in (A.5). Hence, infinite SAM matrices can be generated while retaining the same PAPR performance.

APPENDIX B

DYNAMIC RANGE OF OFDM SIGNAL AMPLITUDE IN CASE 4

The data symbols modulated by *M*-PSK or *M*-QAM is defined as $\underline{X} = [X(0), X(1), ..., X(N-1)]^T$. After applying the proposed SAM method in case 4 along with IFFT operation, the average power of OFDM signal $\underline{x}$ is derived as

$$\begin{aligned} \overline{P}_x &= E\left[(\underline{x})^H (\underline{x}) \right] \\ &= E\left[\left(C^{-1} \underline{X} \right)^H \left(C^{-1} \underline{X} \right) \right] \\ &= E\left[\underline{X}^H \left(C^{-1} \right)^H C^{-1} \underline{X} \right] \\ &= E\left[\underline{X}\, \underline{X}^H \right] I \\ &= E\left[\underline{X}\, \underline{X}^H \right] \end{aligned} \tag{B.1}$$

When substituting the basis sequence defined in equation (5.29), (5.30) and (5.31,) the amplitude of the n^{th} component in the OFDM frame vector, which is employed case 4, is calculated and derived as

$$
\begin{aligned}
\left|x(n)\right| &= \left|\underline{S}^{\langle n\rangle}\cdot\underline{X}^{T}\right| = \left|\sum_{k=0}^{N-1} S^{\langle n\rangle}(k)\cdot X(k)\right| \\
&= \left|s_0^{\langle n\rangle} X(n) + s_1^{\langle n\rangle} X\left(\left(n+N/2\right)\bmod N\right)\right| \\
&= \left|\frac{\alpha}{\sqrt{\alpha^2+\beta^2}}\cdot\exp\left(j\theta_0^{\langle n\rangle}\right)\tilde{X}_0 + \frac{\beta}{\sqrt{\alpha^2+\beta^2}}\exp\left(j\theta_1^{\langle n\rangle}\right)\cdot\tilde{X}_1\right| \\
&= \frac{1}{\sqrt{\alpha^2+1}}\left|\alpha\left|\tilde{X}_0\right|\exp\left[j\left(\theta_0^{\langle n\rangle}+\angle\tilde{X}_0\right)\right] + \left|\tilde{X}_1\right|\exp\left[j\left(\theta_1^{\langle n\rangle}+\angle\tilde{X}_1\right)\right]\right| \\
&= \frac{\left|\tilde{X}_1\right|}{\sqrt{\alpha^2+1}}\left|\alpha\frac{\left|\tilde{X}_0\right|}{\left|\tilde{X}_1\right|}\exp\left[j\left(\theta_0^{\langle n\rangle}-\theta_1^{\langle n\rangle}+\angle\tilde{X}_0-\angle\tilde{X}_1\right)\right]+1\right| \\
&= \frac{\left|\tilde{X}_1\right|}{\sqrt{\alpha^2+1}}\left|\alpha\frac{\left|\tilde{X}_0\right|}{\left|\tilde{X}_1\right|}\exp\left[j\left(\Delta\theta^{\langle n\rangle}+\Delta\angle\tilde{X}\right)\right]+1\right|.
\end{aligned}
\tag{B.2}
$$

When data symbols are *M*-PSK modulated, these conditions yields constant amplitudes such that $\left|\tilde{X}_0\right| = \left|\tilde{X}_1\right| = \overline{P}_x = 1$. Since $\Delta\theta^{\langle n\rangle} \in \{\pm\pi/2, \pm 3\pi/2\}$ were given in Section 5.3.4, and the phase differences between arbitrary two data symbol alphabets is $\Delta\angle\tilde{X} \in \{0, \pi/2, \pi, 3\pi/2\}$, the phase addition of these two alphabets is always in the phase set, as a result of $\Delta\theta^{\langle n\rangle} + \Delta\angle\tilde{X} \in \{0, \pi/2, \pi, 3\pi/2\}$. Correspondingly the exponent value of the phase summation turns to be $\exp\left[j\left(\Delta\theta^{\langle n\rangle}+\Delta\angle\tilde{X}\right)\right] \in \{1, j, -1, -j\}$.

Therefore, the amplitude of the OFDM frame for *M*-PSK, as defined in (B.2), yields

$$
\begin{aligned}
|x(n)| &= \frac{\left|\tilde{X}_1\right|}{\sqrt{\alpha^2+1}}\left|\alpha\frac{\left|\tilde{X}_0\right|}{\left|\tilde{X}_1\right|}\exp\left[\, j\left(\Delta\theta^n+\Delta\angle\tilde{X}\right)\right]+1\right| \\
&= \frac{\sqrt{\overline{P}_x}}{\sqrt{\alpha^2+1}}\left|\alpha\cdot\exp\left[\, j\left(\Delta\theta^n+\Delta\angle\tilde{X}\right)\right]+1\right| \\
&= \begin{cases} \dfrac{\alpha+1}{\sqrt{\alpha^2+1}}\sqrt{\overline{P}_x} & \Delta\theta^n+\Delta\angle\tilde{X}=2d\pi \\ \dfrac{\alpha-1}{\sqrt{\alpha^2+1}}\sqrt{\overline{P}_x} & \Delta\theta^n+\Delta\angle\tilde{X}=(2d+1)\pi \\ \sqrt{\overline{P}_x} & \Delta\theta^n+\Delta\angle\tilde{X}=(2d+1)\pi/2 \end{cases}, \\
& d\in\mathbb{Z}^+, d=0,1,...
\end{aligned}
\tag{B.3}
$$

Accordingly, the peak power of the OFDM signal becomes

$$
\begin{aligned}
&\max_{n=0,1,...,N-1}\left|x(n)\right|^2 \\
&= \max_{n=0,1,...,N-1}\left\{\frac{\overline{P}_x}{\alpha^2+1}\left|\alpha\cdot\exp\left[\, j\left(\Delta\theta^n+\Delta\angle\tilde{X}\right)\right]+1\right|^2\right\} \\
&= \frac{\overline{P}_x}{\alpha^2+1}\left|\alpha\cdot\exp\left[\, j\left(\Delta\theta^n+\Delta\angle\tilde{X}\right)\right]+1\right|^2_{\Delta\theta^{\langle n\rangle}+\Delta\angle\tilde{X}=2d\pi} \\
&= \frac{(\alpha+1)^2}{\alpha^2+1}\overline{P}_x \xrightarrow{\alpha=\infty} \overline{P}_x.
\end{aligned}
\tag{B.4}
$$

Note that the peak power happens at the moment when $\Delta\theta^n+\Delta\angle\tilde{X}=2d\pi$ and obtains the value of $(\alpha+1)\sqrt{\overline{P}_x}\Big/\sqrt{\alpha^2+1}$. In practical application, the maximum amplitude difference depends on the symbol alphabets that data vector contains. (B.4) provides the theoretical peak power boundaries for *M*-PSK modulated signals.

The function of (B.4) with $\overline{P}_x=1$ for *M*-PSK is plotted in Figure B.1. It can be seen that when $\alpha=100$, the peak power of OFDM signal is converging and approaching

to the design objective, as the ideal case of constant power of OFDM signals, with *M*-PSK modulated symbol alphabets.

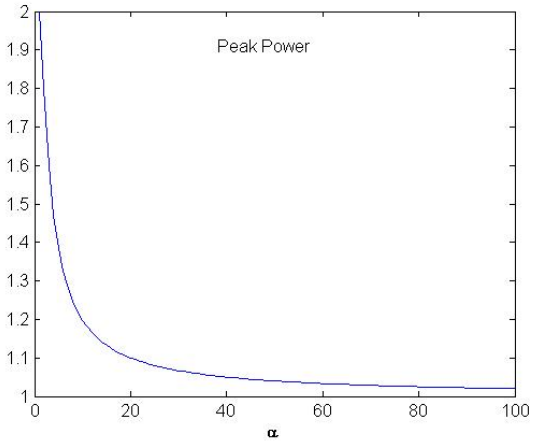

Figure B.1 Peak power of the OFDM frame with case 4 for *M*-PSK.

Besides, for *M*-QAM modulated symbols, when two constellation alphabets, $\left|\tilde{X}_0\right|$ and $\left|\tilde{X}_1\right|$, involve the phase difference of $\Delta\angle\tilde{X} = -\Delta\theta^{\langle n\rangle} \in \{\pm\pi/2, \pm 3\pi/2\}$ and meanwhile the amplitudes of $\left|\tilde{X}_0\right| = \left|\tilde{X}_1\right| = \max_{k=0,1,\ldots,N-1}\left(\left|X(k)\right|\right)$, the peak power boundary of OFDM signals can be estimated as

$$\begin{aligned}
&\max_{n=0,1,\ldots,N-1}\left|x(n)\right|^2 = \max_{n=0,1,\ldots,N-1}\left|\frac{\left|\tilde{X}_1\right|}{\sqrt{\alpha^2+1}}\left|\alpha\frac{\left|\tilde{X}_0\right|}{\left|\tilde{X}_1\right|}\exp\left[\,j\left(\Delta\theta^{\langle n\rangle}+\Delta\angle\tilde{X}\right)\right]+1\right|^2 \\
&= \frac{1}{\alpha^2+1}\left|\alpha\left|\tilde{X}_0\right|\cdot\exp\left[\,j\left(\Delta\theta^{\langle n\rangle}+\Delta\angle\tilde{X}\right)\right]+\left|\tilde{X}_1\right|\right|^2_{\substack{\Delta\theta^{\langle n\rangle}+\Delta\angle\tilde{X}=2d\pi \\ \left|\tilde{X}_0\right|=\left|\tilde{X}_1\right|}} \qquad \text{(B.5)} \\
&= \frac{(\alpha+1)^2\left|\tilde{X}_0\right|^2}{\alpha^2+1} \xrightarrow{\alpha=\infty} \left|\tilde{X}_0\right|^2 = \max\left(\left|X(k)\right|^2\right).
\end{aligned}$$

As aforementioned, the equation (B.5) calculates the theoretical highest boundary for the peak power of data symbols modulated by *M*-QAM. In practical application, the peak power may be smaller than that boundary depending on the actual data symbols. From equation (B.5) it can be observed that as the value of parameter α increases, the peak power of the signal is also minimized, and the boundary of peak power is close to the known maximum value of data symbol alphabets modified by *M*-QAM.

REFERENCES

[1] A. N. Akansu, P. Duhamel, X. M. Lin and M. de Courville, "Orthogonal transmultiplexers in communication: a review," *IEEE Trans. on Signal Processing*, Special Issue on Theory and Applications of Filter Banks and Wavelets, vol. 46, no. 4, pp. 979-995, Apr. 1998.

[2] R. A. Haddad and A. N. Akansu, *Multiresolution Signal Decomposition: Transforms, Subbands, and Wavelets*, Boston, Massachusetts: Academic Press, 1992.

[3] A. N. Akansu and H. Agirman-Tosun, "Generalized discrete Fourier transform with nonlinear phase," *IEEE Transactions on Signal Processing*, vol. 58, no. 9, pp. 4547-4556, Sep. 2010.

[4] A. N. Akansu, H. Agirman-Tosun, and M. U. Torun, "Optimal design of phase function in generalized DFT," *Physical Communication, Elsevier*, vol. 3, no. 4, pp. 255-264, Dec. 2010.

[5] V. Britanak, "A unified discrete cosine and discrete sine transform computation," *Signal Processing, EURASIP*, vol. 43, no. 3, pp. 333-339, May 1995.

[6] A. Jain, "A sinusoidal family of unitary transforms," *IEEE Transactions on Pattern Analysis and Machine Intelligence*, vol. PAMI-1, no. 4, pp. 356-365, Oct. 1979.

[7] E. Fishler, A. M. Haimovich, R. S. Blum, L. J. Cimini, D. Chizhik, and R. A. Valenzuela, "Spatial diversity in radars-models and detection performance," *IEEE Transactions on Signal Processing*, vol.54, no. 3, pp. 823-838, March 2006.

[8] A. M. Haimovich, R. S. Blum, and L. J. Cimini, "MIMO radar with widely separated antennas," *IEEE Signal Processing Magazine*, vol.25, no. 1, pp. 116-129, 2008.

[9] L. Auslander and R. Tolimieri, "Characterizing the radar ambiguity functions," *IEEE Transactions on Information Theory*, vol.30, no. 6, pp. 832-836, Nov. 1984.

[10] N. Levanon, "Multifrequency complementary phase-coded radar signal," *IEE Proceedings-Radar*, Sonar, Navig., vol.147, no. 6, pp. 276-284, Dec. 2000.

[11] N. Levanon and E. Mozeson, *Radar Signals*, Hoboken, NJ: J. Wiley, 2005.

[12] I. Oppermann, “Orthogonal complex-valued spreading sequences with a wide range of correlation properties,” *IEEE Trans. on Communications*, vol. 45, pp. 1379-1380, Nov. 1997.

[13] W. Y. Zou and Y. Wu, “COFDM: An overview,” *IEEE Trans. Broadcast.*, vol. 41, no. 1, pp. 1-8, Mar. 1995.

[14] E. Costa, M. Midro, and S. Pupolin, “Impact of amplifier nonlinearities on OFDM transmission system performance,” *IEEE Communications Letters*, vol. 3, no. 2, pp. 37-39, Feb. 1999.

[15] D. Lim, S. Heo, and J. No, “An overview of peak-to-average power ratio reduction schemes for OFDM Signals,” *Journal of Commun. and Netw.*, vol. 11, no. 3, pp. 229-239, Jun. 2009.

[16] H. Ochiai and H. Imai, “Performance of the deliberate clipping with adaptive symbol selection for strictly band-limited OFDM systems,” *IEEE Journal on Selected Areas in Communications*, vol. 18, no. 11, pp. 2270-2277, Nov. 2000.

[17] S. M. Ju and S. H. Leung, “Clipping on COFDM with phase on demand,” *IEEE Communications Letters*, vol. 7, no. 2, pp. 49-51, Feb. 2003.

[18] G. L. Ren, H. Zhang, and Y. L. Chang, “A complementary clipping transform technique for the reduction of peak-to-average power ratio of OFDM system,” *IEEE Trans. Consumer Electronics*, vol. 49, no. 4, pp. 922-926, Nov. 2003.

[19] J. Davis and J. Jedwab, “Peak-to-mean power control in OFDM, Golay complementary sequences, and Reed-Muller codes,” *IEEE Transactions on Information Theory*, vol. 45, no. 7, pp. 2397-2417, Nov. 1999.

[20] K. Yang and S. Chang, “Peak-to-average power control in OFDM using standard arrays of linear block codes,” *IEEE Communications Letters*, vol. 7, no. 4, pp. 174-176, Apr. 2003.

[21] T. Jiang and G. X. Zhu, “Complement block coding for reduction in peak-to-average power ratio of OFDM signals,” *IEEE Communications Magazine*, vol. 43, no. 9, pp. S17-S22, Sep. 2005.

[22] R. W. Bauml, R. F. H. Fischer, and J. B. Huber, “Reducing the peak-to-average power ratio of multicarrier modulation by selected mapping,” *IEE Electronic Letters*, vol. 32, no. 22, pp. 2056–2057, Oct. 1996.

[23] S. Y. Le Goff, K. K. Boon, C. C. Tsimenidis, and B. S. Sharif, “A novel selected mapping technique for PAPR reduction in OFDM systems,” *IEEE Trans. Comm.*, vol. 56, no. 11, pp. 1775-1779, Nov. 2008.

[24] S. H. Muller and J. B. Huber, “OFDM with reduced peak-to-average power ratio by optimum combination of partial transmit sequences,” *Elect. Lett.*, vol. 33, no. 5, pp. 368-369, Feb. 1997.

[25] L. J. Cimini Jr and N. Sollenberger, “Peak-to-average power ratio reduction of an OFDM signal using partial transmit sequences,” *IEEE Communications Letters*, vol. 4, no. 3, pp. 86-88, Mar. 2000.

[26] A. D. S. Jayalath and C. Tellambura, “Adaptive PTS approach for reduction of peak-to-average power ratio of OFDM signal,” *Electronics Letters*, vol. 36, no. 14, pp. 1226-1228, Jul. 2000.

[27] J. Tellado, “Peak to average power reduction for multicarrier modulation,” Ph.D. dissertation, Stanford University, 2000.

[28] M. Deumal, A. Behravan, and L. Pijoan, “On cubic metric reduction in OFDM systems by tone reservation,” *IEEE Trans. Commun.*, vol. 59, no. 6, pp. 1612-1620, Jun. 2011.

[29] T. Wattanasuwakull and W. Benjapolakul, “PAPR reduction for OFDM transmission by using a method of tone reservation and tone injection,” *in Proc. 5th International Conference on Information, Communications and Signal Processing*, pp. 273-277, Dec. 2005.

[30] S. H. Han, J. M. Cioffi, and J. H. Lee, “Tone injection with hexagonal constellation for peak-to-average power ratio reduction in OFDM,” *IEEE Commun. Lett.*, vol. 10, no. 9, pp. 646-648, Sep. 2006.

[31] B. S. Krongold and D. L. Jones, “PAR reduction in OFDM via active constellation extension,” *IEEE Trans. Broadcast.*, vol. 49, no. 3, pp. 258-268, Sep. 2002.

[32] A. Saul, “Generalized active constellation extension for peak reduction in OFDM systems,” *in Proc. IEEE ICC*, vol. 3, pp. 1974-1979, 2005.

[33] H. Breiling, S. Muller-Weinfurtner, and J. Huber, “SLM peak-power reduction without explicit side information,” *IEEE Communications Letters*, vol. 5, no. 6, pp. 239-241, Jun. 2001.

[34] T. Kojima, S. Iwamoto, Y. Shida, and T. Fujino, “A novel SLM PAPR reduction of OFDM signals without side information,” *IEEE International Symposium on Signal Proc. and Information Tech. (ISSPIT)*, pp. 321-325, Dec. 2010.

[35] S. Su, C. Lee, C. Lin, and Y. Lin, “A novel PAPR reduction scheme without side information by using linear phase rotation vector,” *IEEE Wireless Comm. Netw. Conf.(WCNC)*, pp. 4048-4052, Apr. 2013.

[36] L. Yang, K. K. Soo, S. Q. Li, and Y. M. Siu, "PAPR Reduction using low complexity PTS to construct of OFDM signals without side information," *IEEE Trans. on Broadcast.*, vol. 57, no. 2, pp. 284-290, Mar. 2011.

[37] M. Sharif, C. Florens, M. Fazel, and B. Hassibi, "Amplitude and sign adjustment for peak-to-average-power reduction," *IEEE Trans. on Comm.*, vol. 53, no. 8, pp. 1243–1247, Aug. 2005.

[38] L. Yang, and E. Alsusa, "Novel low-complexity post-IFFT PAPR reduction technique by utilizing amplitude transforming for OFDM systems," *IEEE Wireless Comm. and Netw. Conf.(WCNC)*, pp. 1339-1343, Mar. 2007.

[39] L. Yang, J. Liu, and L. Zhang, "Low-complexity time domain PAPR mitigation by amplitude modification for OFDM systems," *IEEE 72th Veh. Tech. Conf.(VTC2000-Fall)*, pp. 1-5, Sep. 2010.

[40] T. Jiang, W. Xiang, P. C. Richardson, J. Guo, and G. Zhu, "PAPR reduction of OFDM signals using partial transmit sequences with low computational complexity," *IEEE Trans. on Broadcast.*, vol. 53, no. 3, pp. 719-724, Sep. 2007.

[41] Y. C. Cho, S. H. Han, and J. H. Lee, "Selected mapping technique with novel phase sequences for PAPR reduction of an OFDM signal," *IEEE 60th Vehi. Tech. Conf. (VTC2004-Fall)*, vol. 7, pp. 4781-4785, Sep. 2004.

[42] Y. W. Wang, Ali N. Akansu, "Low-complexity peak-to-average power ratio reduction method for orthogonal frequency division multiplexing communications," *IET Communications*, vol. 9, no. 17, pp. 2153-2159, Nov. 2015.

[43] K. M. Yew, M. Drieberg, V. Jeoti, "On PAPR reduction in OFDM systems: a technique using normalized complex Hadamard transform," *TENCON 2005 IEEE Region 10*, pp. 21-24, Nov. 2005.

[44] R. A. Horn and C. R. Johnson, *Topics in Matrix Analysis*, Cambridge, United Kingdom: Cambridge University Press, 1991.

[45] J. Walsh, "A closed set of normal orthogonal functions," *American Journal of Mathematics*, vol. 45, no. 1, pp. 5-24, Jan. 1923.

[46] R. L. Frank, S. A. Zadoff and R. Heimiller, "Phase shift pulse codes with good periodic correlation properties", *IRE Transactions on Information Theory*, vol. 8, no. 6, pp. 381-382, Oct. 1961.

[47] B. L. Lewis and F. F. Kretschmer, "A new class of polyphase pulse compression codes and techniques," *IRE Trans. Inf. Aerospaceand Electronic Systems*, vol. AES-17, no. 3, pp. 364–371, May 1981.

[48] B. L. Lewis and F. F. Kretschmer, "Linear frequency modulation derived polyphase pulse compression codes," *IRE Trans. Inf. Aerospaceand Electronic Systems*, vol. AES-18, no. 5, pp. 637–641, Sept. 1982.

[49] D. Brandwood, *Fourier Transforms in Radar and Signal Processing*, Boston, Massachusetts: Artech House, 2012.

[50] J. A. Nelder and R. Mead, "A simplex method for function minimization," *Computer Journal*, vol. 7, no. 4, pp. 308-313, 1965.

[51] Y. W. Wang, Ali N. Akansu, and Alexander M. Haimovich, "Generalized DFT waveforms for MIMO radar," *Sensor Array and Multichannel Signal Processing Workshop (SAM)*, pp. 301-304, Jun. 2012.

[52] S. M. Sascha, I. Scott and M. Stephen, "An FFT-based approach for fast acquisition in spread spectrum communication systems," *Wireless Personal Communications*, vol. 13, no. 1-2, pp. 27-56, May 2000.

[53] B. Liu, Y. Pi, X. Yang, R. Min and W. Wu, "A novel approach to improve Doppler tolerance of polyphase code," *International Conference on Communications, Circuits and Systems (ICCCAS)*, vol. 1, pp. 558-561, Jul. 2009.

[54] R. A. Stirling-Gallagher, A. P. Hulbert and G. J. R. Povey, "A fast acquisition technique for a direct sequence spread spectrum signal in the presence of a large Doppler shift," *Proceedings of the IEEE Int. Symposium on Spread Spectrum Techniques and Applications*, vol. 1, pp. 156-160, Sep. 1996.

[55] Y. W. Wang and A. N. Akansu, "Generalized DFT based partial matched filter bank for Doppler estimation," *Information Sciences and Systems (CISS)*, pp. 1-6, Mar. 2012.

[56] M. Blachman, "The output signals and noise from a nonlinearity with amplitude-dependent phase shift," *IEEE Trans. Inf. Theory*, vol. 25, pp. 77-79, Jan. 1979.

[57] P. Kaur and R. Singh, "Complementary cumulative distribution function for performance analysis of OFDM signal," *IOSR Journal of Elec. and Commun. Engineering (IOSRJECE)*, vol. 2, no. 5, pp. 5-7, Sep. 2012.

[58] M. Sharif, C. Florens, M. Fazel, and B. Hassibi, "Amplitude and sign adjustment for peak-to-average-power reduction," *IEEE Trans. Commun.*, vol. 53, no. 8, pp. 1243-1247, Aug. 2005.

[59] S. H. Muller and J. B. Huber, "A comparison of peak power reduction schemes for OFDM," *in Proceeding of IEEE Global Telecommunications Conference*, vol. 1, pp. 1-5, Nov. 1997.

[60] K. Atkinson, *An Introduction to Numerical Analysis*, New York City, New York: John Wiley & Sons Press, 1989.

[61] R. A. Brualdi, *Combinatorial Matrix Classes*, pp.19, Cambridge, United Kingdom: Cambridge University Press, 2006.

[62] B. Miklos, *Combinatorics of Permutations*, Boca Raton, Florida: Chapman and Hall-CRC Press, 2004.

[63] G. B. Folland, *Real Analysis: Modern Techniques and Their Applications*, Hoboken, New Jersey: John Wiley & Sons Press, 1999.

[64] J. W. Demmel, *Applied Numerical Linear Algebra*, section 1.7, Philadelphia, Pennsylvania: SIAM Press, 1997.

[65] D. Chu, "Polyphase codes with good periodic correlation properties (Corresp.)," *IEEE Transactions on Information Theory*, vol. 18, no. 4, pp. 531-532, Jul. 1972.

[66] E. Costa, M. Midrio, and S. Pupolin, "Impact of amplifier nonlinearities on OFDM transmission system performance," *IEEE Commun. Lett.*, vol. 3, no. 2, pp. 37-39, Feb. 1999.

[67] S. M. Alamouti, "A simple transmit diversity technique for wireless communications," *IEEE J. Select. Areas Commun.*, vol. 16, no. 10, pp. 1451-1458, Oct. 1998.

[68] E. S. Hassan, S. E. El-Khamy, M. I. Dessouky, S. A. El-Dolil and F. E. Abd El-Samie, "Peak-to-average power ratio reduction in space-time block coded multi-input multi-output orthogonal frequency division multiplexing systems using a small overhead selective mapping scheme," *IET Communications*, vol.3, no. 10, pp. 1667-1674, Oct. 2009.

[69] T. Jiang, C. Ni and L. Guan, "A novel phase offset SLM scheme for PAPR reduction in Alamouti MIMO-OFDM systems without side information," *IEEE Signal Proc. Letters*, vol.20, no. 4, pp. 383-386, Apr. 2013.

[70] W. Rudin, *Principles of mathematical Analysis*, New York City, New York: McGraw-Hill Press, 1976.